NAME: **Naomi Gooden**

YEAR: **Year 4**

Report: **CH401 Research Project**

TITLE: **Nanoparticle Platform for Colourimetric Detection of**

Glycosyl Transferase Activity

SUPERVISOR: **Professor Matthew I. Gibson**

REPORT TYPE: **Standard (8,500 words)**

NUMBER OF WORDS: **9177**

Abstract

Understanding the importance of protein post-translational modifications in neurological disorders could be fundamental for the establishment of effective diagnostic tools and improving current treatment methods. In particular, elucidation of the protein glycosylation changes that take place in Alzheimer's Disease could be instrumental in aiding the development of therapies targeted at preventing or minimising the disease in its early stages.

Glycan-functionalised gold nanoparticles have been explored as a potentially highly sensitive tool for probing the specificity of carbohydrate-protein interactions, exploiting the characteristic optical properties of gold nanoparticles and the ease of surface modification with glycans. Detection of analytes in colourimetric sensing assays is mediated through lectin-induced aggregation of gold nanoparticles, facilitating easy and sensitive recognition of carbohydrate-lectin binding interactions. Glycosyl transferase enzymes involved in characteristic glycosylation pathways in Alzheimer's Disease can be studied using this colourimetric assay approach, eliminating the need for fluorescent-labelling approaches or the expensive analytical procedures commonly required for protein detection.

Herein, a simplistic, label-free colourimetric assay is employed to detect glycosyl transferase enzyme activity, using a model enzyme as a proof of concept study for the development of low-cost, point-of-care biosensors for detection of glycosyl transferase enzymes in Alzheimer's Disease.

Acknowledgements

I would like to express my deepest thanks to my supervisor, Professor Matthew Gibson for providing me with the opportunity to undertake such an exciting and challenging project and for providing me with constant support throughout the project.

I would also like to say a special thank you to my mentor, Sarah-Jane Richards for her endless support and assistance.

Finally, I would like to thank all members of the Gibson research group for always being willing to answer any questions I had in the lab and providing such a friendly, welcoming environment to work in.

List of abbreviations

AD	Alzheimer's Disease
APP	Amyloid precursor protein
AuNP	Gold nanoparticle
Aβ	Amyloid-β peptide
CSF	Cerebrospinal fluid proteins
CTA	Chain transfer agent
DP	Degree of polymerisation
GlycoAuNP	Glycosylated gold nanoparticle
MS	Mass spectroscopy
PFP	Pentafluorophenol
pHEA	Poly(hydroxyethyl acrylamide)
PNA	Peanut Agglutinin
RAFT	Reversible Addition-Fragmentation Chain Transfer
RCA	*Ricinus communis* Agglutinin I
SBA	Soybean Agglutinin
SEC	Size exclusion chromatography
SPR	Surface plasmon resonance
ST	Sialyltransferase enzyme
TEM	Transmission electron microscopy
UEA	*Ulex europaeus* Agglutinin
WGA	Wheat Germ Agglutinin

Contents

1 Introduction

1.1 Background of Alzheimer's Disease

1.1.1 The pathological cascade of Alzheimer's Disease

Neurological disorders are conditions affecting the function of the nervous system, resulting from damage to the brain, spine or nerves. Alzheimer's Disease (AD) is the most common neurological disorder, affecting almost 30 million people worldwide, and this figure is predicted to quadruple by 2050.[1] Development of effective treatments for AD has been a prominent research topic for many years, with the only treatments currently available targeting the symptoms caused by the disease. With the rapid expected increase in people suffering from AD, there is a pressing need to develop treatments which minimise or prevent the disease and diagnostic tools for earlier disease detection.

It is widely known that two of the key pathological changes that take place during the progression of AD are the build-up of amyloid plaques and neurofibrillary tangles in the brain.[1,2] The exact role of amyloid plaques and neurofibrillary tangles in relation to the disease is not clear, but it is still important to study them to gain a better understanding. Amyloid plaques are formed by the deposition of amyloid-β peptide (Aβ), which is generated from the amyloid precursor protein (APP) through the action of protease enzymes β-secretase and γ-secretase. Neurofibrillary tangles are formed by an accumulation of hyperphosphorylated tau protein.[3]

1.1.2 Protein glycosylation in Alzheimer's Disease

Protein post-translational modifications determine the functions of proteins and have a crucial role in the development of the nervous system and in neurodegeneration.[4] Phosphorylation is the most studied post-translational modification, but in different tissues in the body, protein glycosylation is estimated to be more prevalent. Unusual protein glycosylation patterns have been identified in several disease states[5] and in particular recent studies have indicated the occurrence of abnormal glycosylation changes in AD.[4,6,7] Focusing research efforts on the importance of post-translational modifications in AD could help improve understanding of the earlier stages of AD, which will facilitate the development of improved biomarkers and treatment methods of the disease.

Glycosylation is an important post-translational modification in AD. This process regulates the amount of presenilin complex component and β-secretase enzyme, which are both involved in cleavage of the APP.[4,6,7] Abnormal glycosylation of the APP and tau protein, two fundamental proteins associated with the pathological cascade of AD, affects

intracellular sorting, processing and exportation of these proteins. The extent of glycosylation is affected by β-secretase and γ-secretase enzymes. In particular, the β-secretase cleaves and generates soluble forms of the otherwise membrane-bound sialyltransferase enzymes (STs).[3]

Figure 1: *N*-Glycosylation of AD-related proteins including the APP and β-secretase enzyme (BACE-1).[8]

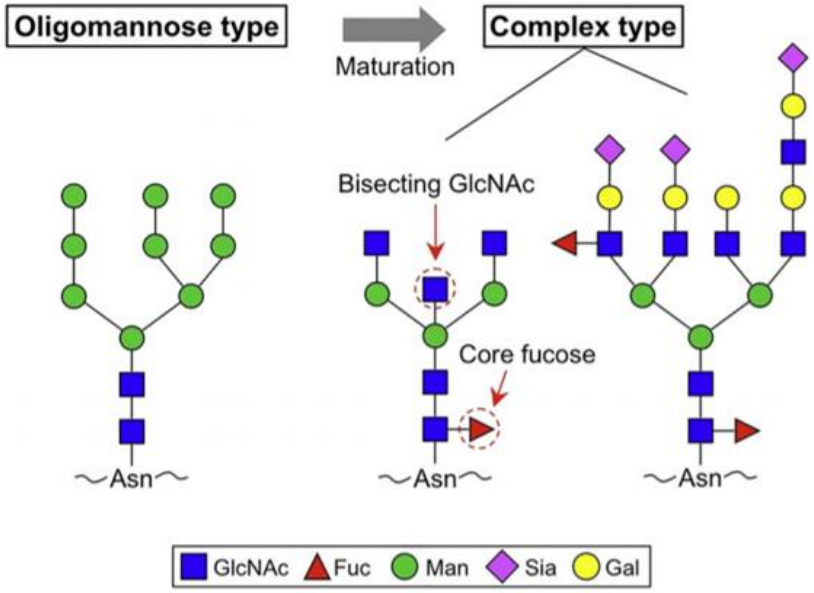

Figure 2: Typical *N*-glycan structures. The glycan building blocks depicted are *N*-acetylglucosamine (GlcNac), fucose (Fuc), mannose (Man), sialic acid (Sia) and galactose (Gal).[8]

Sialyltransferase enzymes catalyse the transfer of sialic acid to glycans. Glycans have many important roles in biological systems and importantly also act as signals to determine how glycoproteins are processed within the cell. The functions of glycoproteins are usually studied by treatment with inhibitors, enzymatic removal and using lectins, which are carbohydrate-binding proteins with a high specificity for specific sugars.[3] Fodero *et al.* used lectins to study the sialylation of cerebrospinal fluid proteins (CSF) in AD.[5] From this study it was identified that there was significantly lower protein sialylation in AD compared with non-AD. The importance of protein sialylation in AD could be investigated by examining sialyltransferases as potential biomarkers.

1.2 Biosensors as a diagnostic tool

Identification of novel biomarkers will help to provide an early indication of many neurodegenerative disorders, such as AD and Parkinson's disease, facilitating the development of treatments to target earlier stages of the disease.[9,10] Currently poor techniques account for many of the challenges in the identification of clinically relevant biomarkers for disease diagnosis, in addition to lack of availability of relevant tissues and the complexity of the brain.[9] Recent research strategies in AD have focused on studying the CSF, with the major advantage being this is a much less invasive sample to obtain in comparison to brain tissue.[11] Aβ in the CSF have been identified as potential biomarkers for AD, using surface plasmon resonance (SPR) biosensors as a technique to investigate their activity.[12,13]

A biosensor is an analytical device which combines a biorecognition element with a transducer. The biorecognition element provides selective or specific binding with target analytes. The transducer component signals the binding event and influences the concentrations the biosensor detects.[14,15] Surface plasmon resonance biosensors rely on an optical transduction component. In general, there are two types of optical detection – labelled and label-free. Labelled detection relies on an evanescent field to excite fluorescent or chemical labels.[16] In comparison, label-free detection does not require chemical or fluorescent labelling of the analyte, and is primarily based upon the refractive index of the detection medium.[17] Gold nanoparticles are commonly used optical biosensors, exploiting the SPR phenomenon on gold surfaces.

1.3 Gold nanoparticles as biosensors

1.3.1 Properties and advantages of gold nanoparticles

Nanomaterials have unique physicochemical properties that can improve the efficiency of biosensors.[15] In particular, AuNPs are commonly used for fabrication of chemical and biological sensors due to their distinctive physical and chemical properties.[15,18,19] The unique optoelectronic properties of AuNPs can be exploited for their use in colourimetric detection sensing assays. Additionally, AuNPs have a high surface-to-volume ratio, they are fairly easy to synthesise and have a good biocompatibility[20]. Perhaps the property which is most advantageous in their applications as biosensors is the ease of functionalisation with an array of organic and biological molecules which facilitates selective binding to target molecules.[21]

1.3.2 Synthesis and surface functionalisation of gold nanoparticles

One of the most commonly applied synthetic approaches is the citrate reduction of $HAuCl_4$ in water. This method was developed by Turkevich in 1951[22], and was further refined by Frens to allow control over NP size.[23]

NP functionalisation involves modification of the NP surface by the addition of a chemical group to the surface. Conjugation with thiols and thiolated ligands is the most common modification, taking advantage of strong Au-S bonds.[24] Although thiol-ligands are the most common, functionalisation with amines, phosphines and carboxylate ligands have also been reported.[25]

There are two main strategies that are applied for the introduction of functional groups to the NP surface – direct and post-functionalisation. Direct functionalisation involves direct attachment of a functional ligand to the surface. The functional ligand consists of two functional groups to allow attachment of one reactive moiety to the NP surface while the other reactive moiety modifies the surface, which facilitates conjugation to the desired target.[26] Post-functionalisation involves initial reaction of a binding-chelating group to the surface, before conversion to the reactive NP surface-modifying group.[27]

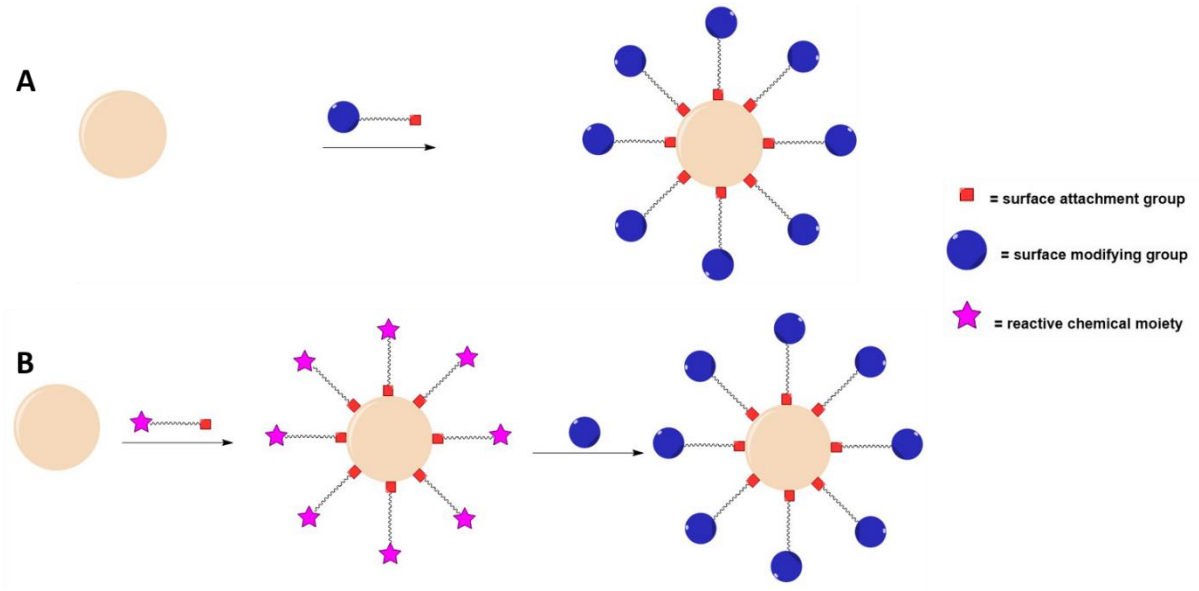

Figure 3: (A) Direct functionalisation, involving direct attachment of the chemical moiety. (B) Post-functionalisation, involving attachment of a ligand containing a reactive chemical end group which is modified by the molecule of interest.

1.3.3 Surface plasmon resonance

AuNPs exhibit surface plasmon resonance, which results from the collective oscillations of the conduction band electrons due to photoexcitation.[28–31] The resonance condition for AuNPs occurs at visible wavelengths, giving rise to an intense colour of the NPs. SPR is influenced by the size, solvent, ligand, interparticle distance and temperature. Monodisperse AuNPs in solution appear red in colour, with the SPR absorbance occurring at ~520 nm. Aggregation of AuNPs reduces the interparticle distance, causing a shift in the resonance condition to between 600 – 700 nm, and a distinctive colour change is observed in the solution from red to blue.[29,30,32] This characteristic has made AuNPs an attractive candidate for use as colourimetric sensors.

1.3.4 Colourimetric detection assays

The colour change that is observed during aggregation of AuNPs provides a basis for the absorbance-based colourimetric sensing of target analytes that trigger aggregation.[33] Typical NP-based biosensors comprise of an immobilised ligand substrate which is structurally modified in the presence of a target analyte. Modification of the substrate causes a change in the environment of the NPs leading to a change in the aggregation status, which results in a visually detectable colour change.[32] Sensitivity of colourimetric assays is dependent on the molar extinction coefficient of the NPs which is affected by material composition and the particle size.[32] The chain length of the anchor group also influences both the sensitivity and stability of NPs in assays. Studies have shown that

ligands with a shorter chain length have improved sensitivity in colourimetric assays, whereas ligands with a longer chain anchor group were seen to form a more stable monolayer.[34]

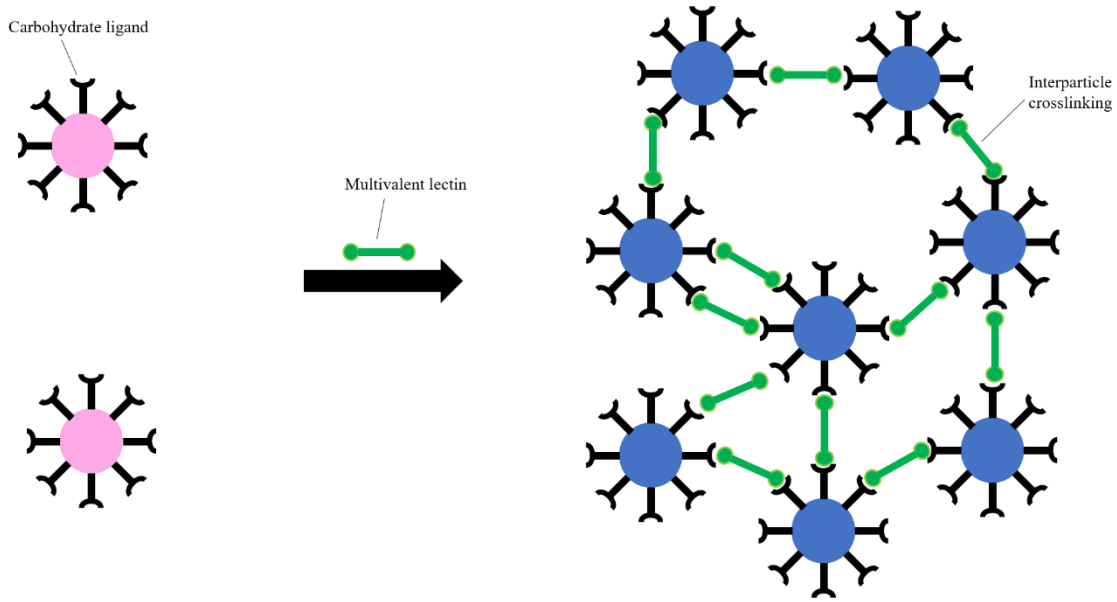

Figure 4: Gold nanoparticle aggregation initiated by multivalent lectin binding inducing colour change from red to blue.

Aggregation can be triggered through both interparticle crosslinking and non-crosslinking means. Interparticle crosslinking causes NP aggregation by forming linkages between individual particles. Linkages can be formed utilising crosslinking molecules, which have two binding sites and are able to link two AuNPs together. This strategy relies on interparticle forces and is limited to analytes that have at least two easily accessible binding sites. Alternatively, NPs can be crosslinked by functionalisation of the AuNPs with two different, complementary ligands.[35,36]

In non-crosslinking AuNP aggregation, aggregation is induced without the formation of interparticle bonds. Instead, aggregation is caused by a stronger interaction between the NP and the target analyte. This strategy is useful for conducting colourimetric assays of enzyme activity, as it is a more rapid detection method which facilitates real-time measurement of enzyme activity.[35,36]

1.3.5 Stabilisation

There have been challenges implementing AuNP sensors in biological applications, due to the destabilisation of NPs that is noted under physiological conditions. The presence of additional salt, DNA and other small molecules in biological fluids affects the aggregation of NPs which influences colourimetric detection assay results.[24,32,33,37] To

improve stability, the AuNP surface can be modified with molecules that interact with the surface through electrostatic or bonding interactions.

Electrostatic stabilisation involves the formation of an electrical double layer by the particles and counter ions in the medium. This stabilises the NPs against van der Waals forces, but is highly sensitive to salt concentration which affects the size of the double layer. Alternatively, ligands that are adsorbed or bound to the surface stabilise NPs by forming a physical barrier across the NP, preventing unwanted aggregation. Steric stabilisation is advantageous in solutions of higher salt concentrations, as the stability is not sensitive to changes in ionic strength.[32]

Uncharged polymer coatings are commonly applied to improve stability. Stabilisation of AuNPs by polymers is precisely controlled by their relative chain length, grafting density and monomer composition. These factors need to be considered and optimised to provide a balance between stability of the NPs in biological media and the speed of colourimetric detection.[34] Additionally, it is important to consider techniques that aim to minimise the dispersity of the polymer mixture. Living polymerisation methods allow the molecular weight and polydispersity of the polymer to be controlled, enabling the production of well-defined polymers.[38] Reversible Addition-Fragmentation Chain Transfer (RAFT) is one of the most promising living polymerisation techniques, as it is a versatile technique and permits the use of a wide range of monomers and functionalities.[39] In RAFT polymerisation, the addition of a chain transfer agent to the system facilitates transfer of the growing polymer chain to the chain transfer agent, which allows a narrow molecular weight distribution of the polymer.[39]

1.4 Colourimetric sensing

1.4.1 Advantages of AuNP colourimetric assays

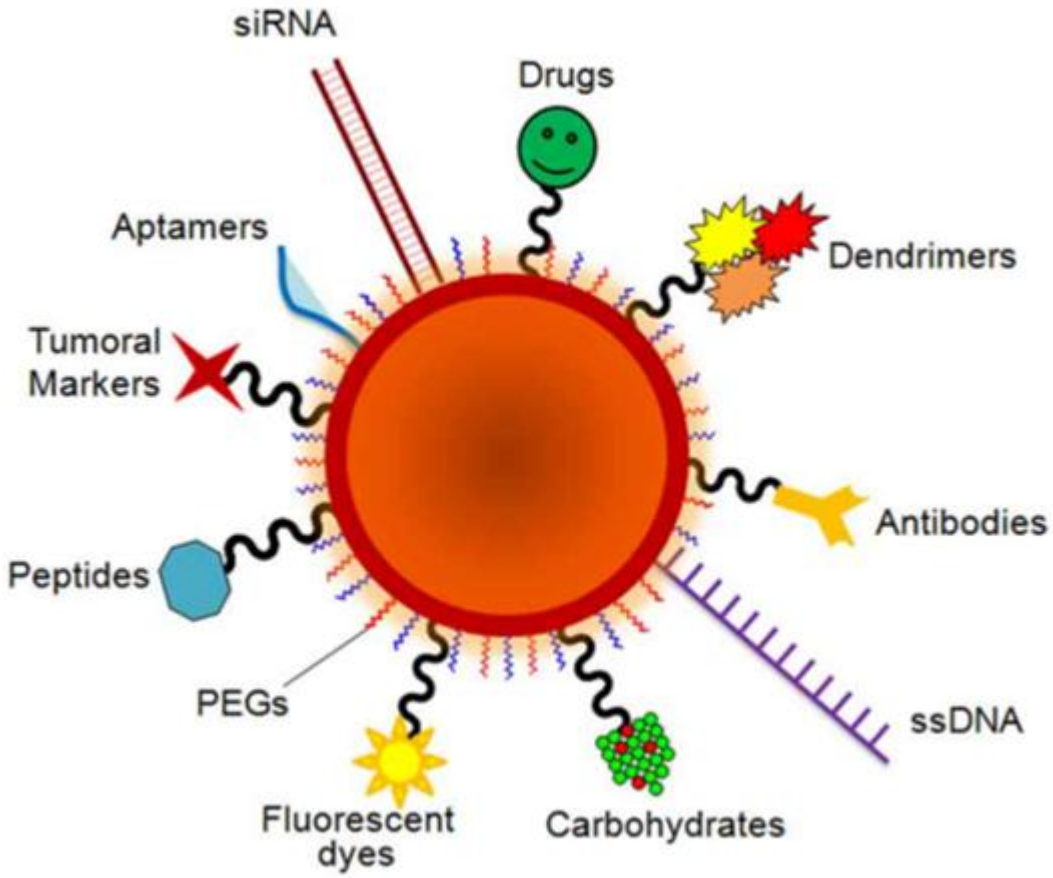

Figure 5: Some examples of different molecules conjugated to NPs.[40]

AuNP-based colourimetric assays have been employed in a broader range of applications in comparison to conventional detection systems. One major advantage is the simplicity of sensing methods without the need for complex instrumentation. The simplicity of the sensing method facilitates the potential application of these systems into point-of-care testing diagnostics.[32] Already, AuNP colourimetric sensing assays have been applied for use in home pregnancy tests[41] and analyses of specific gene sequences[42] as well as detection of other target analytes.

1.4.2 Colourimetric assay examples

Mirkin and coworkers have developed some of the most widely used AuNP-based colourimetric assay sensing systems utilising DNA oligonucleotide strands conjugated with the NPs.[43–45] DNA – AuNP colourimetric assays have been conducted for detection of a range of analytes that are fundamental to biological systems.

One example Mirkin *et al.* pioneered was the detection of cysteine via a DNA – AuNP colourimetric approach[43] which was found to be a much simpler alternative to more widely used cysteine detection techniques.[46,47] Other examples discuss the detection of metal ions,[45] oligonucleotides[44] and cancerous cells.[48]

Sensitive detection of proteins could be highly important for certain diseases in which the presence of specific protein biomarkers or irregular protein concentrations are indicative of the disease. AuNPs have been applied for colourimetric detection of proteins via different strategies. Aptamer-based strategies combine the high affinity and selectivity of aptamers with the spectroscopic advantages of AuNPs.[32,33] Other studies have detailed the synthesis of carbohydrate-functionalised AuNPs, which are utilised for the detection of carbohydrate binding proteins and for studying carbohydrate-protein interactions.[15]

1.4.3 Glyconanoparticles for colourimetric detection

Developing tools to progress knowledge and understanding of carbohydrate-protein interactions is fundamental due to the importance of carbohydrates in biological systems. Carbohydrate-carbohydrate interactions are involved in processes such as metastasis and fertilisation.[28,34] Carbohydrate-protein interactions mediate processes such as cell-cell signalling, inflammation and fertilisation.[28,34] There have also been studies that have shown that the interactions that take place between carbohydrates and bacteria/virus/toxins on cell surfaces can mediate infections. Having a deeper understanding of this interaction could facilitate the development of more targeted therapies to improve the treatment of infections.

The ease of functionalisation of the NP surface facilitates the use of carbohydrate-functionalised AuNPs as an alternative tool to well-established techniques such as carbohydrate microarrays and carbohydrate-modified polymers for studying carbohydrate-protein interactions.[28] Carbohydrate-functionalised AuNP colourimetric assays combine the optical properties of AuNPs with the specific analyte targeting of the carbohydrate ligand.[28,34,49] Manipulation of the glyco-AuNP conjugate properties, such as the carbohydrate ligand used and the chain length of the anchor group, enables selective tailoring of colourimetric assays to achieve sensitive detection of biological targets.

The carbohydrate-NP conjugate can be assembled by either direct self-assembly of the carbohydrate ligand onto the NP surface, or by functionalisation of the AuNPs with a non-glyco ligand, then reacting the AuNP-non-glyco ligand conjugate with a carbohydrate.[34]

Colourimetric assays using carbohydrate-functionalised NPs can be employed to monitor carbohydrate-protein interactions by using lectins.[49,50]Although most carbohydrate-protein interactions are weak, this is overcome in nature through multivalent binding, which gives rise to a stronger total binding affinity than the binding affinity to each individual carbohydrate, this is known as the 'cluster-glycoside effect'.[51,52] The multivalency of lectins is exploited in colourimetric detection assays to crosslink nanoparticles, triggering aggregation.

Detection of enzymes using AuNP colourimetric assay techniques is advantageous for studying enzyme activity and monitoring enzyme-catalysed reactions. Nanosensors have already been developed for studying hydrolysases and proteases. The development of sensitive colourimetric assay techniques for studying sialyltransferase enzyme activity could be useful for both understanding the importance of protein sialylation in AD and potentially for use as a diagnostic technique.

1.5 Aims and objectives

The facile conjugation of glycans with AuNPs for colourimetric detection assays with lectins has been previously detailed as discussed above. This work aims to utilise this foundation to explore the binding interaction between lactosamine- and sialyllactosamine-functionalised Au NPs and lectins and to identify lectins that exhibit a different binding response for both sugars. Using this knowledge, the central focus is to construct a simplistic, sensitive colourimetric assay utilising lactosamine-functionalised Au NPs for the detection of α-2,3-sialyltransferase enzyme activity, with the potential for employment of the colourimetric sensing system as an enzymatic biosensing tool.

2 Experimental

2.1 Materials

Acetone, dichloromethane, toluene, methanol, diethyl ether and hydrochloric acid were purchased from Fischer Scientific. Potassium phosphate tribasic (≥ 98 %), dodecane thiol (≥ 98 %), carbon disulfide (≥ 99 %), *N*-(3-dimethylaminopropyl)-*N*′-ethylcarbodiimide hydrochloride (≥ 98 %), *N*-hydroxyethyl acrylamide (97 %), mesitylene (98 %), 4,4′-azobis(4-cyanovaleric acid) (98 %), sodium chloride, sodium citrate, triethylamine (99%), tetrachloroauric acid, Tris base, cytidine-5′-monophospho-*N*-acetylneuraminic acid and α-2,3-sialyltransferase enzyme from *Pasteurella multocida* were all purchased from Sigma-Aldrich. Pentafluorophenol and 4-(dimethylamino)pyridine were purchased from Acros. Lactose was purchased from Fluka. 2,3-sialyllactose was purchased from Carbosynth. Peanut agglutinin (PNA), wheat germ agglutinin (WGA), *Ricinus communis* agglutinin I (RCA), soybean agglutinin (SBA) and *Ulex europaeus* agglutinin (UEA) lectins were purchased from Vector Labs and made into 2 $mg.mL^{-1}$ solutions in HEPES buffer immediately before use. The HEPES buffer that was used contained: 0.05 M NaCl, 0.1 mM $CaCl_2$ and 0.01 mM $MnCl_2$ (pH 7.5 HEPES). Clear, polystyrene, flat-bottom, half-area 96-well microtitre plates were purchased from Greiner Bio-one.

2.2 Physical and Analytical Methods

^{1}H and ^{13}C NMR spectra were recorded using a Bruker DPX-300 or Bruker DPX-400 NMR Spectrometer. Chemical shifts are reported in ppm (δ) relative to the deuterated solvent used. Spectra were analysed using ACD/Labs 1D NMR Processor. Mass spectrometry was performed in methanol on the Agilent 6130B ESI-Quad instrument using electrospray in positive and negative ion mode. SEC measurements were carried out on an Agilent 390-LC MDS system equipped with a PL-gel 5μm guard column, two PL-gel Mixed D columns (300 x 7.5 mm) equipped with a differential refractive index, viscometry, dual angle light scatter and UV detectors. DMF was used as the eluent at a flow rate of 1 mL min^{-1} at 50˚C. Data were analysed using Agilent GPC/SEC software and molecular weight determined relative to narrow molecular weight PMMA standards (200 – 1.0 x 106 g mol^{-1}). UV-Vis absorbance measurements were recorded on a BioTek Synergy HT Multidetection Microplate reader using Gen5 1.11 multiple data collection and analysis software. DLS measurements were carried out using a Malvern Instruments Zetasizer Nano-ZS.

2.3 Synthetic Procedures

2.3.1 Synthesis of RAFT agent PFP-DMP

Synthesis of 2-(dodecylthiocarbonothioylthio)-2-methylpropionic acid (DMP)

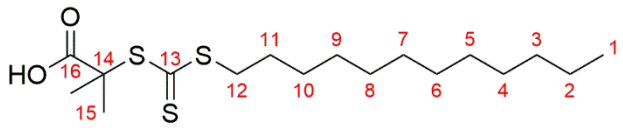

Figure 6: ^{12}C labelled DMP structure.

DMP was synthesised according to a modified procedure of Phillips *et. al.*[53]

A suspension of K_3PO_4 (4.2 g, 20 mmol) in acetone (60 mL) was stirred at room temperature for 25 minutes, while adding dodecane thiol (4.0 g, 20 mmol) dropwise. On addition of CS_2 (4.1 g, 54 mmol) the solution changed colour to yellow. The solution was stirred for ten minutes before addition of 2-bromo-2-methylpropionic acid (3.0 g, 18 mmol). A precipitation of KBr was observed and the solution was left stirring overnight at room temperature. The solvent was removed *in vacuuo* and the residue was extracted into DCM (2 x 200 mL) from 1 M HCl (200 mL), before washing with water (200 mL) and brine (200 mL) and drying over $MgSO_4$. The solvent was removed under reduced pressure and the residue was purified by recrystallisation, yielding a yellow powder product (1.43 g, 19.8%).

^{1}H NMR (400 MHz, $CDCl_3$) δ_{ppm}: 7.26 ($CDCl_3$); 3.28 (2H, t, J = 7.5 Hz, H^{12}); 1.73 (6H, s, H^{15}); 1.26 (20H, s, H^2 – H^{11}); 0.90 (3H, t, J = 6.7 Hz, H^1).

^{13}C NMR (400 MHz, $CDCl_3$) δ_{ppm}: 220.9 (C^{13}); 177.7 (C^{16}); 77.3, 77.0, 76.7 ($CDCl_3$); 55.5 (C^{14}); 37.1 (C^{12}); 31.9, 29.6, 29.5, 29.4, 29.1, 29.0, 27.8 (C^3 – C^{11}); 25.3 (C^{15}); 22.7 (C^2); 14.1 (C^1).

MS (ESI) m/z: 363.0 $[M-H]^-$; expected 364.2 ($C_{17}H_{32}O_2S_3$).

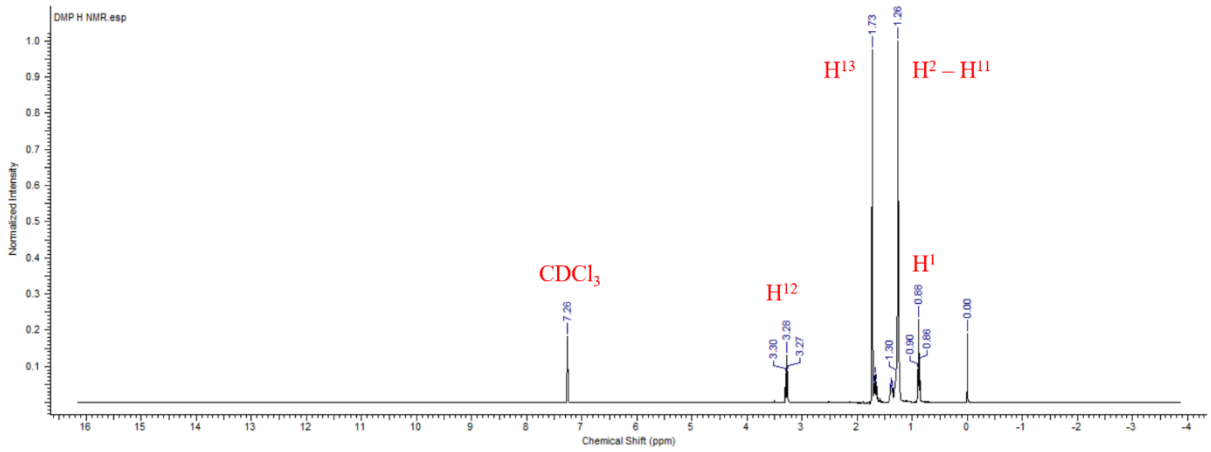

Figure 7: Labelled ^{1}H NMR spectrum of DMP.

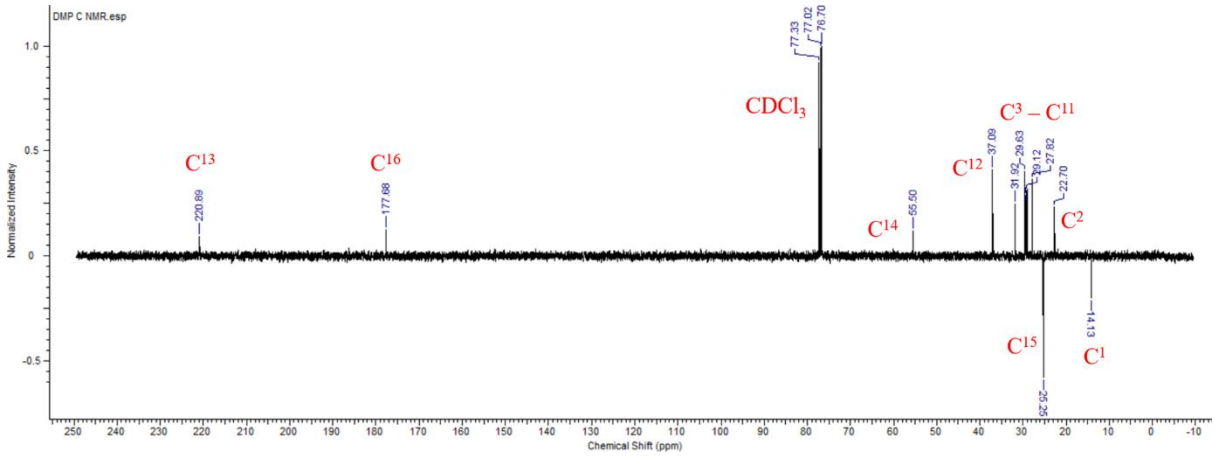

Figure 8: Labelled ^{13}C NMR spectrum of DMP.

Synthesis of pentafluorophenyl 2-(dodecylthiocarbonothioylthio)-2-methylpropionic acid (PFP-DMP)

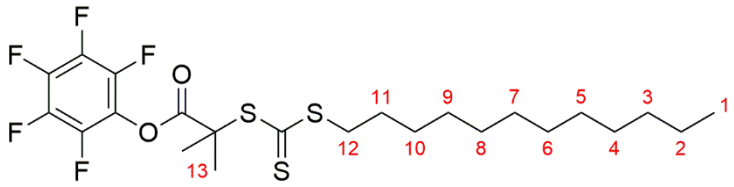

Figure 9: ^{1}H labelled structure of PFP-DMP.

PFP-DMP was synthesised according to the procedure of Richards *et al.*[49]

DMP (0.5 g, 1.4 mmol), *N*-(3-dimethylaminopropyl)-*N′*-ethylcarbodiimide hydrochloride (EDC) (0.39 g, 2.0 mmol), and 4-(dimethylamino)pyridine (DMAP) (0.25 g, 2.0 mmol) were dissolved in DCM (40 mL) and the solution was stirred for 20 minutes under N_2 gas. A solution of pentafluorophenol (0.78 g, 4.2 mmol) in DCM (5 mL) was added and

the reaction was stirred overnight at room temperature. The residue was washed with 3 M HCl, 1 M $NaHCO_3$ and 0.5 M NaCl successively, before drying over $MgSO_4$ and concentration of the residue *in vacuuo* to yield a yellow oil (0.5 g, 68.8 %).

^{1}H NMR (400 MHz, $CDCl_3$) δ_{ppm}: 3.24 (2H, t, J = 7.4 Hz, H^{12}); 1.79 (6H, s, H^{13}); 1.18 (20H, s, $H^{2\text{-}11}$); 0.80 (3H, t, J = 6.7 Hz, H^1).

MS (ESI) m/z: 531.1 $[M+H]^+$; expected 530.1 ($C_{23}H_{31}F_5O_2S_3$).

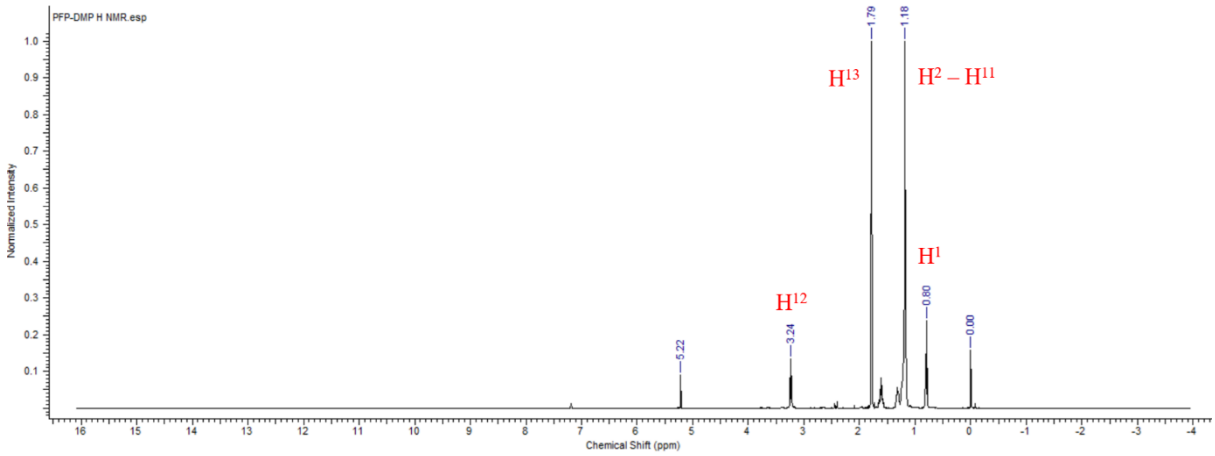

Figure 10: Labelled ^{1}H NMR spectrum of PFP-DMP.

2.3.2 Polymerisation of hydroxyethyl acrylamide (HEA) using PFP-DMP

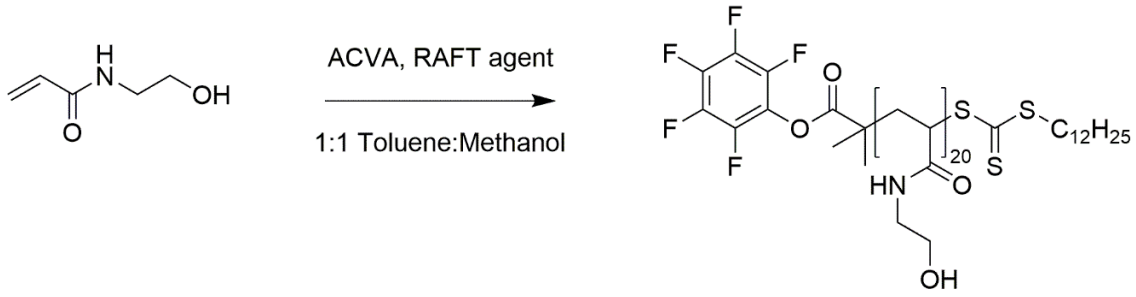

Scheme 1: Polymerisation of hydroxyethyl acrylamide using the PFP-DMP chain transfer agent.

N-Hydroxyethyl acrylamide (HEA) (0.5 g, 4.4 mmol), pentafluorophenyl 2-(dodecylthiocarbonothioylthio)-2-methylpropionic acid (PFP-DMP) (0.115 g, 0.2 mmol) and 4,4′-Azobis(4-cyanovaleric acid) (ACVA) (0.0122 g, 0.04 mmol) were dissolved in a solution of 50:50 toluene:methanol (4 mL). Mesitylene (150 µL) was added to the solution as an internal reference. After this addition, an aliquot of the solution was taken for NMR analysis in $CDCl_3$. After 30 minutes of stirring under N_2 gas, the reaction was

heated to 70°C and stirred at high heat for 90 minutes. An aliquot of the solution was then taken for NMR analysis in MeOD. After rapid cooling of the reaction in liquid nitrogen, the solution was precipitated into diethyl ether. The polymer was reprecipitated from methanol into diethyl ether and dried under vacuum, which yielded the yellow polymer product, PFP-poly(hydroxyethyl acrylamide) (PFP-pHEA). The polymer was characterised using SEC in DMF. 85 % conversion by NMR, M_n (Theoretical) = 2800 g mol^{-1}, M_n (SEC) = 2500 g mol^{-1}, M_w/M_n (SEC) = 1.17.

^{1}H NMR (400 MHz, MeOD) δ_{ppm}: 8.07 (1H, br. s, N*H*); 4.70 (MeOD); 3.60 (2H, m, CH_2OH); 3.49 (2H, m, CH_2NH); 3.25 (1H, m, C*H*-CONH); 3.17 (2H, m, CH_2CHS); 2.23 (2H, m, CH_2S); 1.56 (6H, s, 2 x CH_3); 1.10 (20 H, s, 10 x CH_2); 0.69 (3H, s, CH_3).

2.3.3 Synthesis of 50 nm gold nanoparticles

Gold nanoparticles were synthesised according to a modified procedure of Bastus *et al.*[23]

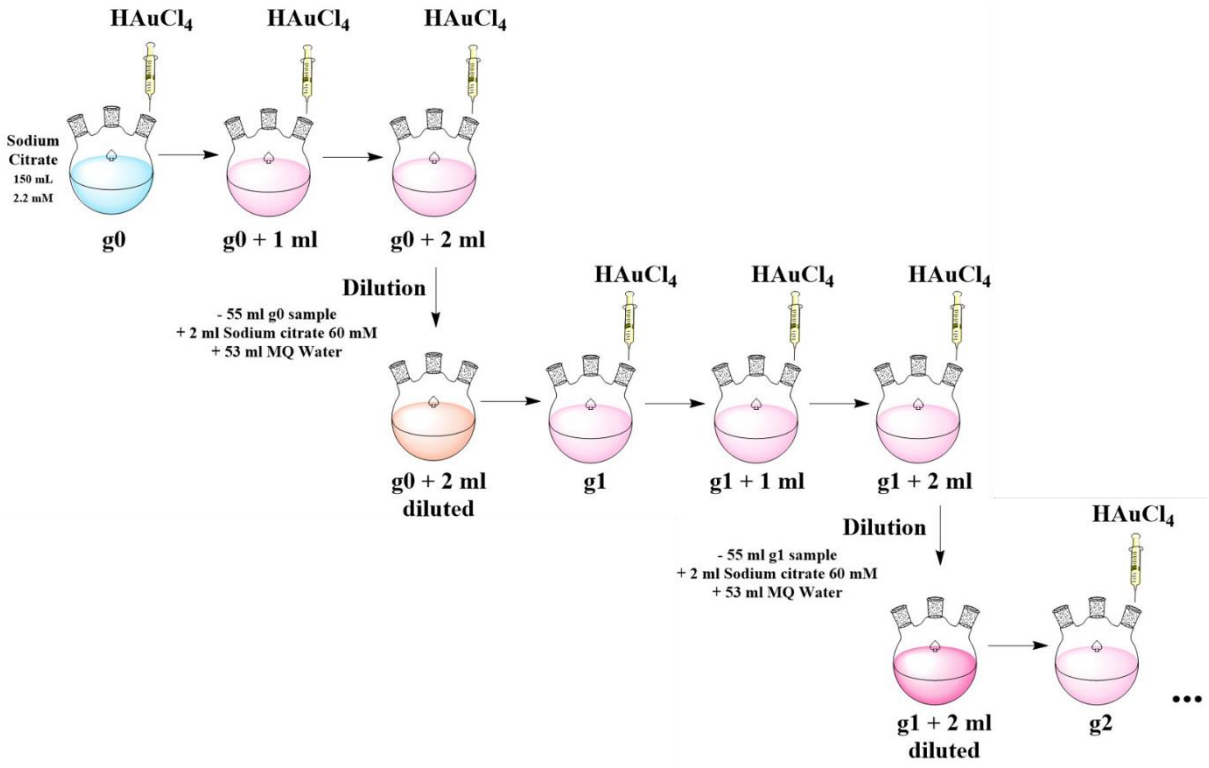

Scheme 2: Seeded growth synthesis of gold nanoparticles, controlling the size of the nanoparticles generated.

Synthesis of Au seeds:

A 2.2 mM solution of sodium citrate in Milli-Q-water was heated to 100˚C in a 250 mL three-necked round-bottomed flask for 15 minutes with vigorous stirring. Once the

solution started boiling, 1 mL of 25 mM $HAuCl_4$ was injected. Over the next 10 minutes, the solution changed colour from yellow to bluish grey to soft pink to dark red.

Seeded growth of AuNPs

After synthesis of the Au seeds, the reaction was immediately cooled until the temperature of the solution reached 90˚C, at which point 1 mL of 25 mM $HAuCl_4$ solution was injected into the reaction mixture. Over the next hour, at each 30-minute interval an additional 1 mL of 25 mM $HAuCl_4$ was injected into the reaction mixture, with continuous stirring throughout the process. After three injections of $HAuCl_4$, 55 mL of the reaction mixture was extracted and replaced with a solution mixture consisting of 53 mL of Milli-Q-water and 2 mL of 60 mM sodium citrate. An aliquot of the solution was taken for analysis by Dynamic Light Scattering (DLS) and UV-Vis spectroscopy to monitor the size of the nanoparticles. To continue the growth of the nanoparticles, 1 mL of 25 mM $HAuCl_4$ was injected in the seed solution and the process was repeated again, until the nanoparticles reached a measured size of 50 nm. Particle size characterised by DLS and UV-Vis (figure 11).

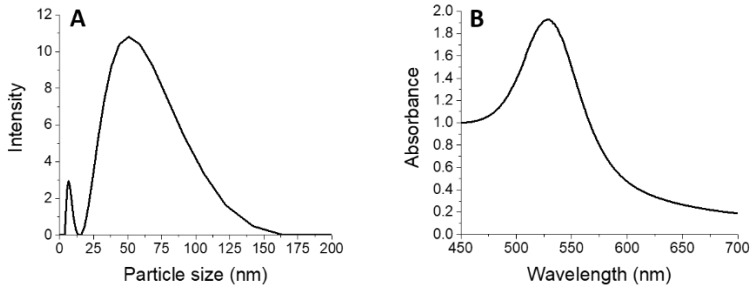

Figure 11: (A) DLS particle size characterisation. Au seed diameter measured as 50 nm. (B) UV-Vis absorption spectrum of AuNPs. Particle size estimated by the method of Haiss *et al.*[54] using the position of the surface plasmon resonance peak (528 nm) which corresponds to diameter size 44 nm.

Table 1: Particle size of each generation of AuNPs as determined by UV-Vis and DLS.

Particle generation	**λ_{spr} (nm)**	**Average diameter size by UV-Vis (nm)**	**Average diameter size by DLS (nm)**
Generation 1	525	32	34
Generation 2	528	44	50

2.3.4 Synthesis of lactosamine-conjugated gold nanoparticles

Synthesis of lactosamine

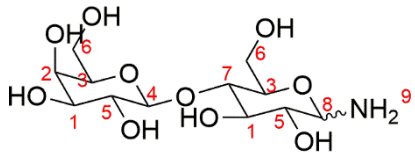

Figure 12: ^{1}H labelled structure of lactosamine.

Lactose (1 g, 2.9 mmol) was added to water (10 mL) and the solution was stirred until dissolved. Ammonium carbonate was added continuously until the solution was saturated. After complete saturation the reaction was left stirring at room temperature for five days until the reaction was fully complete by MS. The residue was dissolved in warm methanol and the product was freeze dried before MS analysis to remove any water, yielding a cream-coloured powder (0.90 g, 90%).

^{1}H NMR (400 MHz, D_2O) δ_{ppm}: 5.14 (1H, d, H^4); 4.70 (D_2O); 4.58 (1H, d, $H^{8\alpha}$); 4.37 (1H, d, $H^{8\beta}$); 4.24 (1H, d, H^9); 4.04 (1H, d, H^9); 3.89 – 3.22 (11H, m, H^1, H^2, H^3, H^5, H^6); 3.12 (2H, t, H^7).

^{13}C NMR (400 MHz, D_2O) δ_{ppm}: 102.9 (C^4); 95.7 (C^8); 86.7 (C^7); 84.9 (C^3); 78.6 (C^3); 75.7 – 68.5 (C^1, C^2, C^5); 61.0 (C^6).

MS (ESI) m/z: 342.2 [$M+H^+$]; expected 341.1 ($C_{12}H_{23}NO_{10}$).

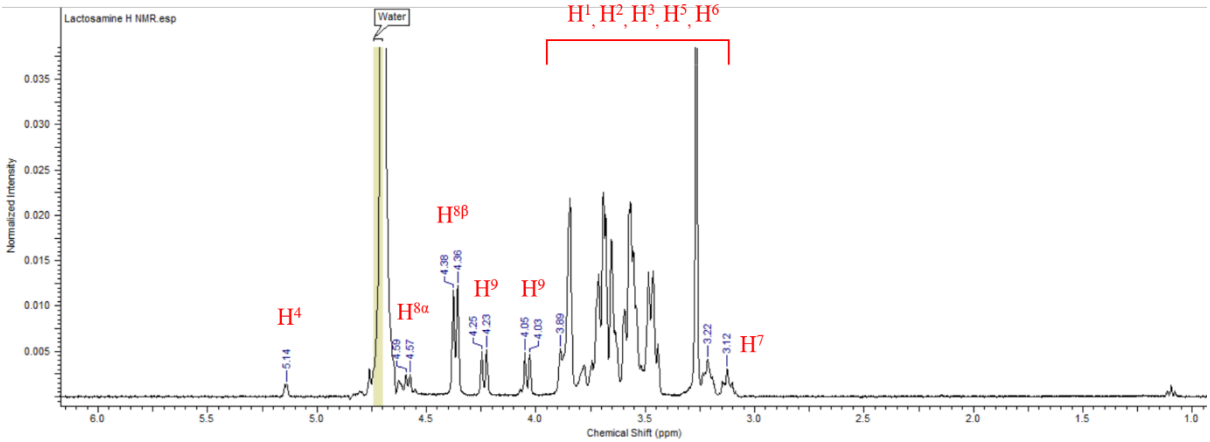

Figure 13: Labelled ^{1}H NMR spectrum of lactosamine.

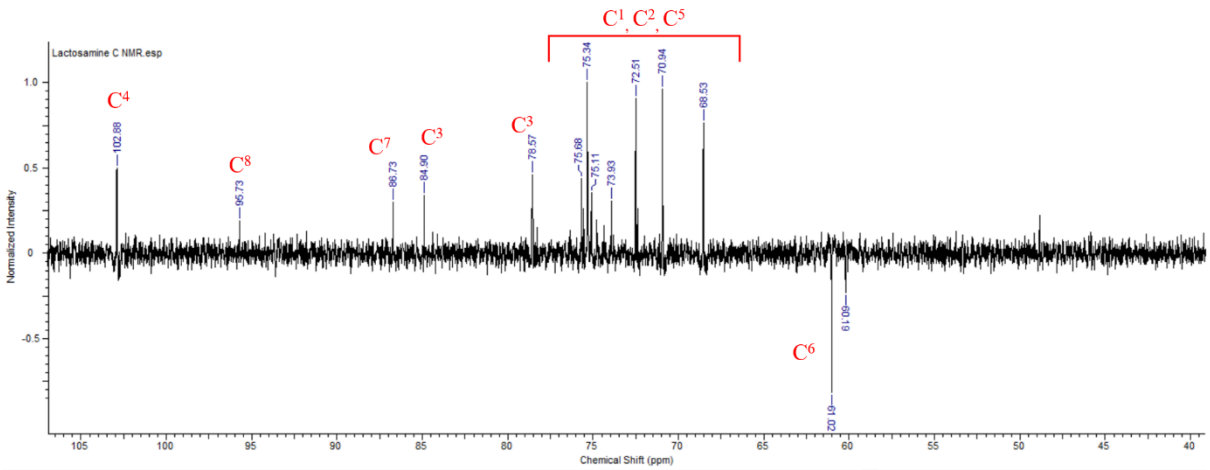

Figure 14: Labelled ^{13}C NMR spectrum of lactosamine.

Synthesis of poly(hydroxyethyl acrylamide)-lactosamine (pHEA-lactosamine)

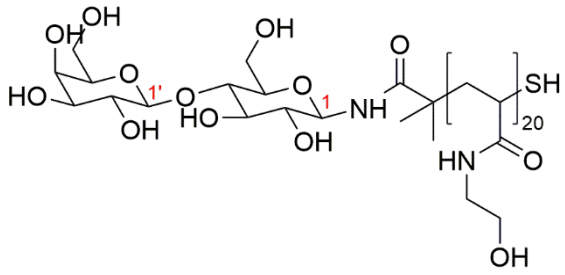

Figure 15: Structure of poly(hydroxyethyl acrylamide)-lactosamine.

PFP-pHEA (80 mg, 0.03 mmol) and lactosamine (50 mg, 0.14 mmol) were dissolved in 2 mL DMF, with the addition of 0.05 M TEA. The reaction was left to stir at room temperature overnight, after which the polymer was precipitated into diethyl ether from methanol twice, dissolved in 5 mL water and freeze dried, to yield a white powder (30 mg).

^{1}H NMR (400 MHz, D_2O) δ_{ppm}: 7.84 (2H, s, 2 x N*H*CO); 5.69 (1H, d, $H^{1'}$); 4.70 (D_2O); 4.61 (1H, d, $H^{1\alpha}$); 4.35 (1H, d, $H^{1\beta}$); 3.45 (2H, m, CH_2OH); 4.2 – 2.6 (all other sugar resonances); 3.25 (2H, m, CH_2NH); 2.92, 2.76 (DMF); 2.59 (1H, m, C*H*-CONH); 2.35 (2H, m, CH_2CHS); 1.09 (3H, s, 2 x CH_3).

Synthesis of polyhydroxyethyl acrylamide-lactosamine nanoparticles

pHEA-lactosamine (1 mg) was dissolved in 50 nm gold nanoparticles (1 mL) and the solution was stirred for 1 hour at room temperature. The solution was centrifuged twice

and the supernatant was removed along with any excess polymer, before resuspension of the particles in water.

2.3.5 Synthesis of sialyllactosamine-conjugated gold nanoparticles

Synthesis of 2,3-sialyllactosamine

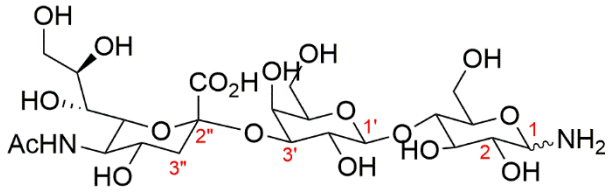

Figure 16: Structure of 2,3-sialyllactosamine.

2,3-sialyllactose (0.1 g, 0.16 mmol) was added to water (10 mL) and the solution was stirred until dissolved. Ammonium carbonate was added continuously until the solution was saturated. After complete saturation the reaction was left stirring at room temperature for five days until the reaction was fully complete by MS. The residue was dissolved in warm methanol and the product was freeze dried before MS analysis to remove any water. The product yielded was a cream-coloured powder (0.24 g).

^{1}H NMR (400 MHz, D_2O) δ_{ppm}: 4.70 (D_2O); 4.63 (2H, d, $H^{1\alpha/\beta}$); 4.44 (1H, d, $H^{1'}$); 4.02 (1H, d, $H^{3'}$); 3.11 (1H, t, H^{2}); 2.67 (1H, dd, $H^{3"eq}$); 1.94 (3H, s, Ac); 1.71 (1H, t, $H^{3"ax}$). All other ^{1}H resonances between 3.87 – 3.26 ppm.

MS (ESI) m/z: $[M+H]^+$ 633.4; expected 632.2 ($C_{23}H_{40}N_2O_{18}$).

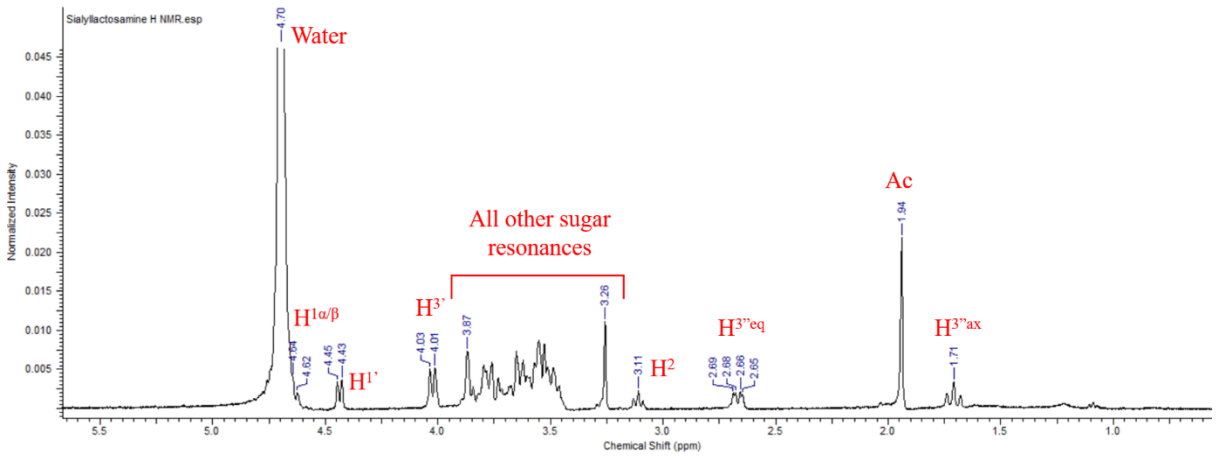

Figure 17: Labelled ^{1}H NMR spectrum of sialyllactosamine.

Synthesis of polyhydroxyethyl acrylamide-sialyllactosamine (pHEA-sialyllactosamine)

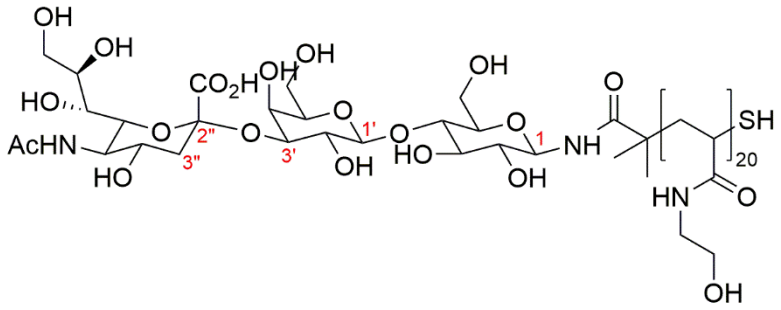

Figure 18: Structure of poly(hydroxyethyl acrylamide)-2,3-sialyllactosamine.

PFP-pHEA (50 mg, 0.018 mmol) and sialyllactosamine (60 mg, 0.088 mmol) were dissolved in 2 mL DMF, with the addition of 0.05 M TEA. The reaction was left to stir at room temperature overnight, after which the polymer was precipitated into diethyl ether from methanol twice. The polymer was dissolved in 5 mL H_2O and the product was freeze dried, to yield a white powder (40 mg).

^{1}H NMR (400 MHz, D_2O) δ_{ppm}: 5.11 (1H, d, $H^{1\alpha}$); 4.69 (D_2O); 4.64 (1H, d, $H^{1\beta}$); 4.43 (1H, d, $H^{1'}$); 4.04 (1H, d, $H^{3'}$); 4.0 – 3.0 all other sugar resonances; 3.58 (2H, m, C*H*$_2$OH); 3.23 (2H, m, C*H*$_2$NH); 2.63 (1H, m, C*H*-CONH); 2.14 (2H, m, C*H*$_2$CHS); 1.94 (3H, s, Ac); 1.53 (6H, br. s, 2 x CH_3).

Synthesis of polyhydroxyethyl acrylamide-sialyllactosamine nanoparticles

pHEA-sialyllactosamine (1 mg) was dissolved in 50 nm gold nanoparticles (1 mL) and the solution was stirred for 1 hour at room temperature. The solution was centrifuged twice, and the supernatant was removed along with any excess polymer, before resuspension of the particles in water.

2.3.6 Enzymatic Assays

Preparation of 0.1 M Tris-HCl pH 8

Tris Base (0.605 g) was dissolved in 30 mL H_2O. Solution was adjusted to pH 8 by the addition of 2.92 mL 0.1 M HCl. After mixing the solution, H_2O was added to make the solution up to 50 mL.

Assays

Lectin induced aggregation studies by absorbance:

A stock solution (2 $mg.mL^{-1}$) of the lectin was prepared in 10 mM HEPES buffer with 0.05 M NaCl, 0.1 mM $CaCl_2$ and 0.01 mM $MnCl_2$. 25 μL serial dilutions of the lectin were prepared in the same buffer in a 96-well micro-titre plate. 25 μL of glycoAuNP were added to each well. Absorbance was measured at 450 nm, 520 nm and 700 nm. An absorbance spectrum was produced after recording measurements at 37˚C every minute for 30 minutes. The spectrum produced was recorded from 450 nm – 700 nm with 10 nm intervals.

Enzymatic assays:

Enzymatic assays were performed in a total reaction volume of 200 μL in Tris-HCl (0.1 M, pH 8) containing cytidine-5′-monophospho-*N*-acetylneuraminic acid (CMP-Neu5Ac) (30 mM), lactosamine (25 mM) and varied quantities of α-2,3-sialyltransferase enzyme (2 μg – 10 μg). Reactions were left at 37˚C for 1 – 6 days. Enzymatic assays that utilised lactosamine dissolved in Tris-HCl were analysed by mass spectroscopy.

Enzymatic assays performed using CMP-Neu5Ac (30 mM), sugar-conjugated AuNPs (25 mM), α-2,3-sialyltransferase enzyme (10 μg) in a total reaction volume of 200 μL in Tris-HCl (0.1 M, pH 8) were left to proceed at 37˚C for 24 h. Results of these assays were analysed by UV-Vis spectroscopy.

Lectin/enzyme induced aggregation studies by absorbance:

A stock solution (2 $mg.mL^{-1}$) of the lectin was prepared in 10 mM HEPES buffer with 0.05 M NaCl, 0.1 mM $CaCl_2$ and 0.01 mM $MnCl_2$. 10 μL 2 × serial dilutions of the lectin were prepared in the same buffer in a 384-well micro-titre plate. 10 μL of glycoAuNP from enzymatic assays were added to each well. Absorbance was measured at 450 nm, 520 nm and 700 nm. An absorbance spectrum was produced after recording measurements at 37˚C every minute for 30 minutes. The spectrum produced was recorded from 450 nm – 700 nm with 10 nm intervals.

3 Results and Discussion

3.1 Synthesis of glycosylated gold nanoparticles

Glycan-functionalised AuNPs comprising of the AuNP, pHEA coating and the glycan were prepared using an optimised synthetic approach designed to generate stabilised conjugates with high sensitivity for application in colourimetric detection assays. The overall approach involved construction of the glycan-polymer conjugate, before direct attachment to the nanoparticle *via* the thiol end group (scheme 3).

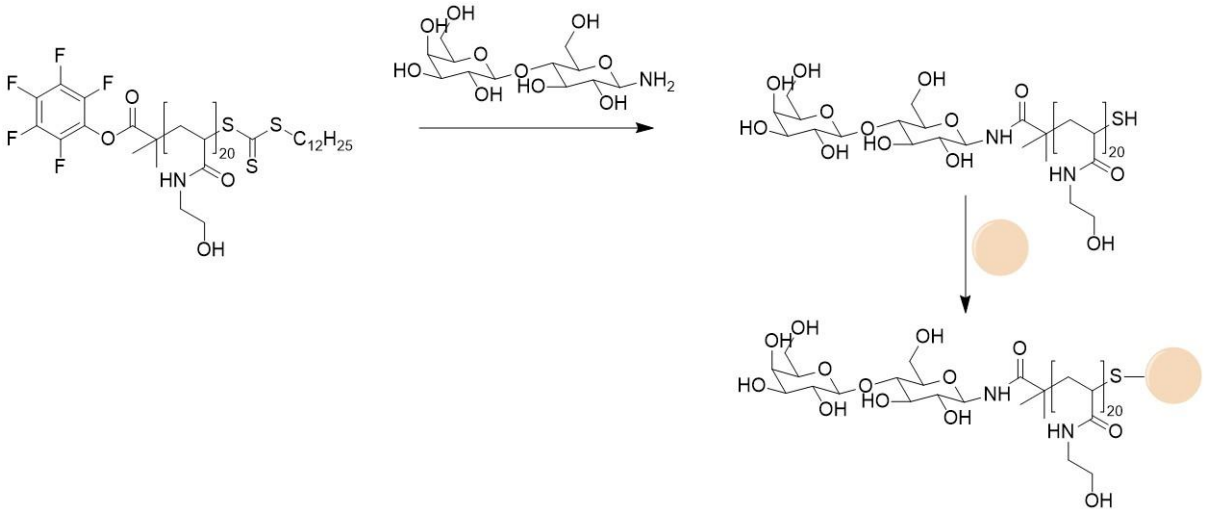

Scheme 3: Gold nanoparticle functionalisation with glycans.

A telechelic polymer was used to enable modification at both ends of the polymer. An amine reactive group at one end facilitates conjugation to the amine moiety of the aminoglycoside *via* the carboxylic acid functional group, and a thiol group at the other end enables attachment to the NP surface as shown in scheme 3.

3.1.1 Synthesis of glycan-linked poly(hydroxyethyl acrylamide)

RAFT polymerisation was employed as this method facilitates the preparation of the desired telechelic polymer, installing latent thiol groups at the chain end for AuNP immobilisation and allowing modification with amino-glycosides at the other end *via* the PFP group. Additionally, RAFT polymerisation allows good molecular weight control.

Hydroxyethyl acrylamide was used as it gives a polymer which is water soluble and has been widely employed for the stabilisation of gold nanoparticles by the GibsonGroup.[49,50,55] Using a monomer : CTA ratio of 20 : 1 allowed targeting the degree of polymerisation (DP) to produce polymers with DP20, as this chain length was

previously found to provide good colloidal stability whilst ensuring rapid responses in colourimetric assays for 40 – 60 nm AuNPs.[49,50] SEC characterisation shows monomodal distribution and a molecular weight of 2500 g mol^{-1} which agrees with the monomer : CTA feed ratio (figure 19).

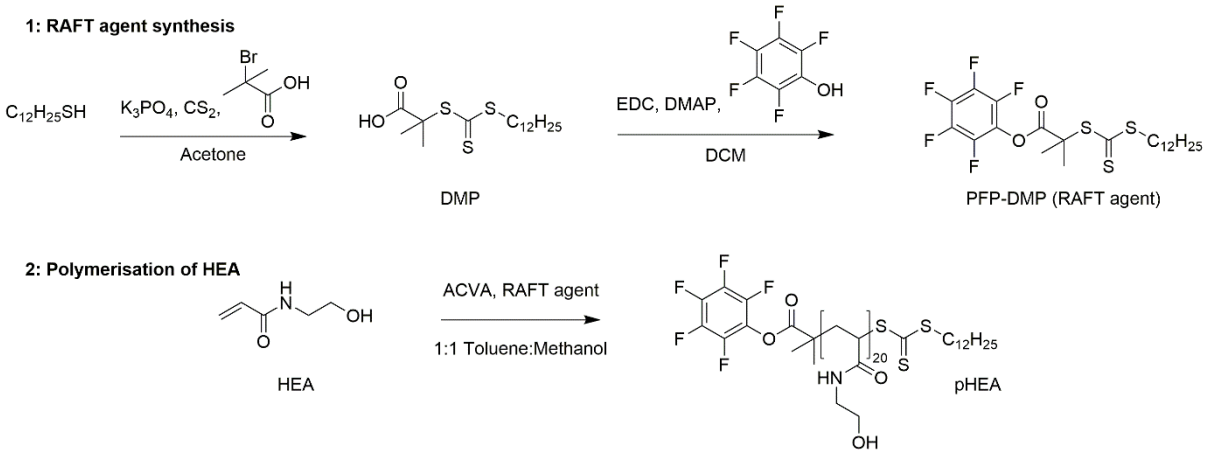

Scheme 4: (1) Synthesis of PFP-DMP chain transfer agent. (2) Polymerisation of hydroxyethyl acrylamide using the chain transfer agent.

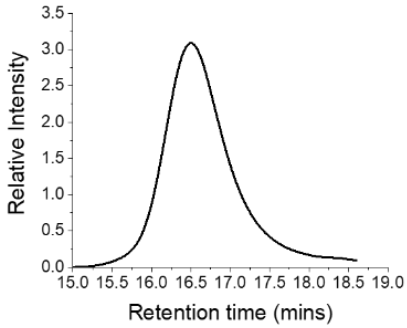

Figure 19: SEC trace of pHEA.

Lactosamine and sialyllactosamine were selected as these sugars are a good model for monitoring sialyltransferase (ST) enzyme activity in colourimetric detection assays. The exposed galactose subunit of lactosamine-functionalised AuNPs is an acceptor of sialic acid, which is transferred from the CMP-sialic acid substrate by the action of ST enzymes as shown in (scheme 5).

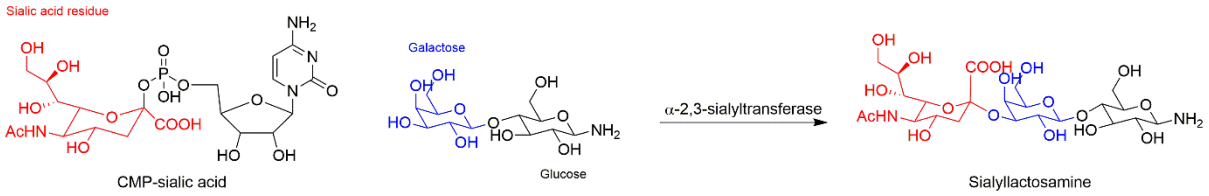

Scheme 5: α-2,3-sialyltransferase mediated sialyllactosamine formation via the transfer of a sialic acid residue (red) from CMP-sialic acid to the terminal galactose subunit (blue) of lactosamine.

The amino functionality is required for AuNP functionalisation. Lactosamine and sialyllactosamine were prepared by direct amidation of the reducing sugars. Saturation of the sugars with ammonium carbonate produced the aminoglycoside, which was characterised by NMR and mass spectroscopy. The reaction proceeded *via* the equilibrium detailed in (scheme 6) favouring formation of the thermodynamically stabilised β-anomer, which is indicated by the relative intensities of the α and β protons in the ^{1}H NMR spectrum in (figure 20). Subsequently, the PFP end-group of pHEA was modified by reaction with the aminoglycosides to produce the polymer-glycan conjugates used to functionalise the AuNP surface.

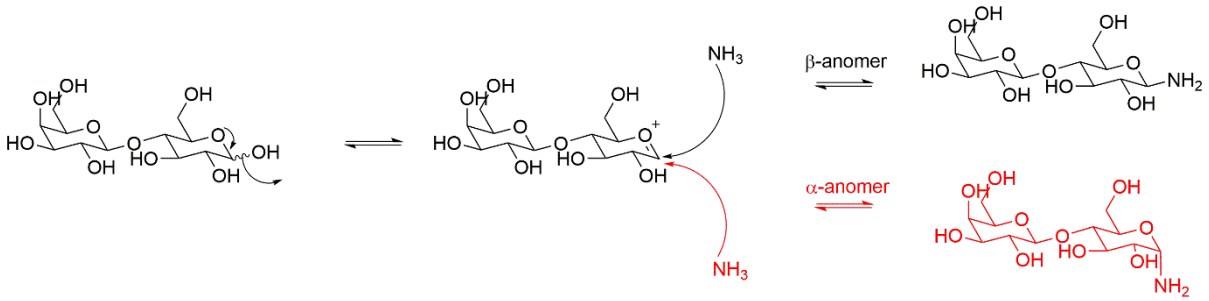

Scheme 6: Synthesis of lactosamine.

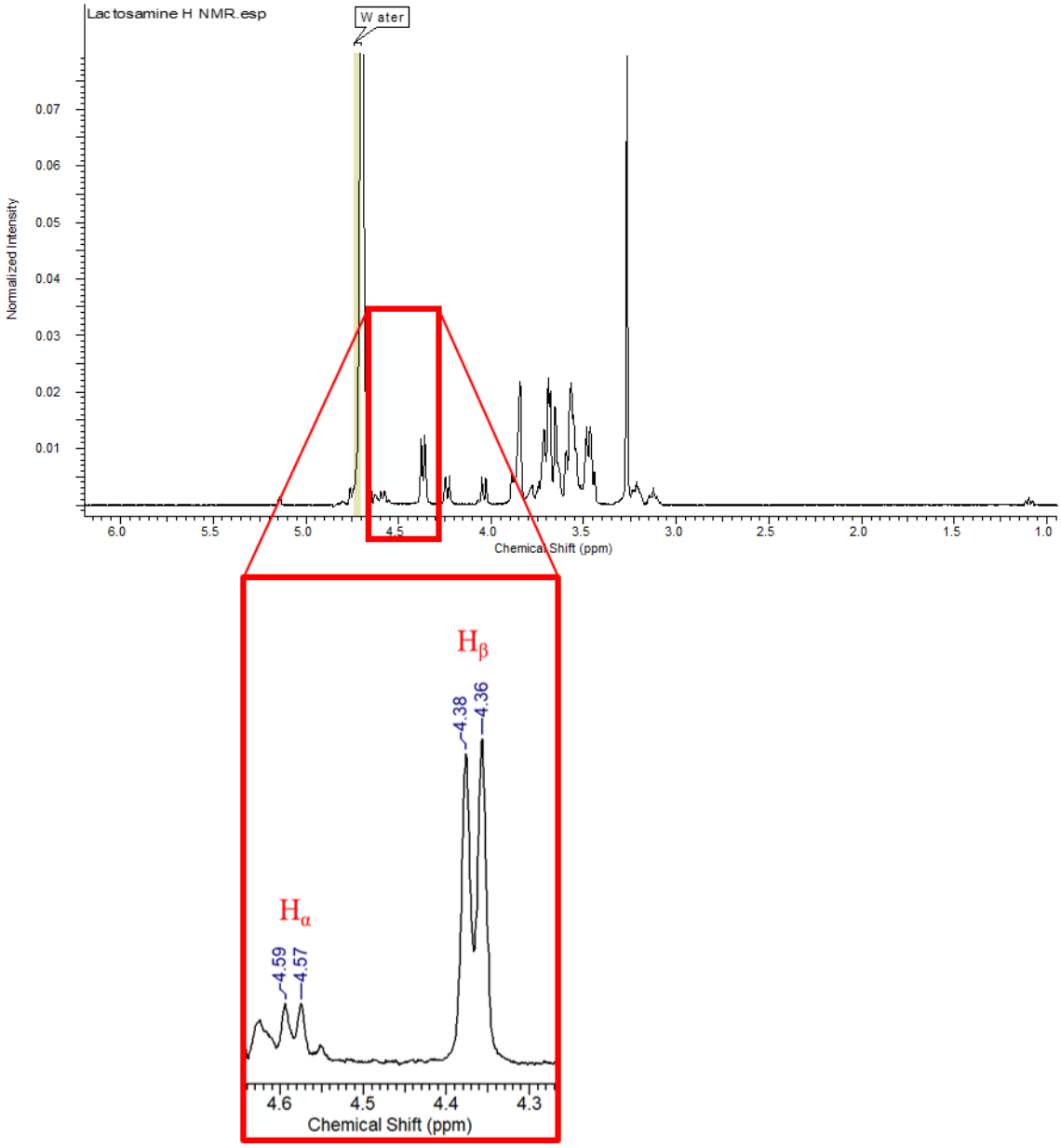

Figure 20: ^{1}H NMR of lactosamine, showing α-proton resonance at 4.58 ppm and β-proton resonance at 4.37 ppm. Higher relative intensity of the β-proton resonance indicates a higher proportion of the β-anomer product.

3.1.2 Preparation of AuNPs

A seeded growth strategy based on the Turkevich/Frens method was employed for synthesis of citrate stabilised AuNPs (see scheme 2), which enables control over the size of NPs formed by varying the feed ratio of $HAuCl_4$ to sodium citrate.[22,23] AuNP synthesis was tuned to produce particles with diameter size 50 nm, using previously published procedures.[23] This size has previous been shown to give improved sensitivity and lower (improved) detection limits.[56]

The size of the nanoparticles was characterised by UV-Vis spectroscopy, DLS and transmission electron microscopy (TEM). Nanoparticle size is correlated to the position of the surface plasmon resonance peak (maximum absorbance in UV-Vis) as previously determined by the work of Haiss et. al.[54] The SPR absorbance of the AuNPs generated was 528 nm, corresponding to a particle diameter size of 44 nm. This corroborates with the diameter measured by DLS, which was determined to be 50 nm. (figure 21) It is worth nothing that the measurements made assume that the nanoparticles are spherical in shape, which is not always true for metallic nanoparticles. TEM of the nanoparticles confirmed the size of the particles to be in the 40 nm range, and that spherical particles were obtained (figure 22).

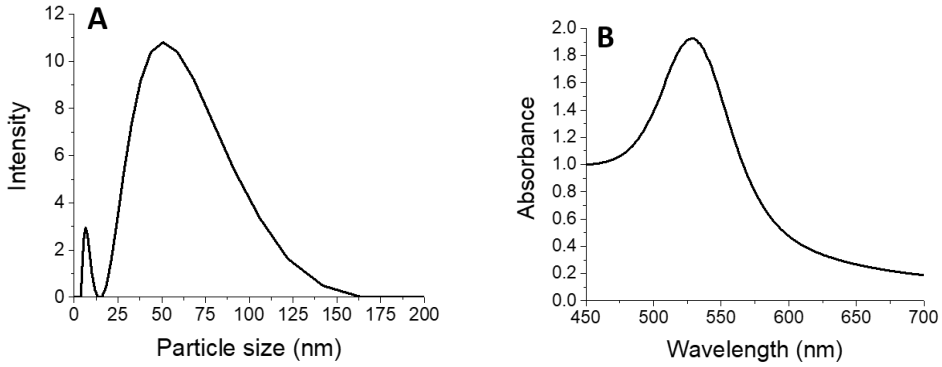

Figure 21: (A) DLS measurement of nanoparticle size. (B) UV-Vis measurement showing surface plasmon resonance peak. The peak position corresponds to diameter size.

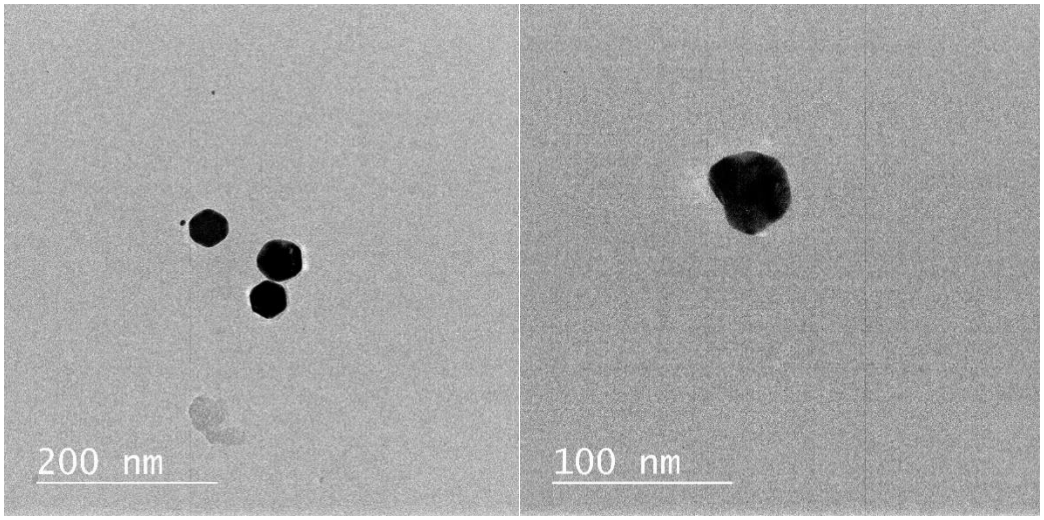

Figure 22: TEM images of AuNPs at 30 000 X (left) and 60 000 X magnification (right).

Following AuNP synthesis and characterisation, the stability of polymer coated versus uncoated particles was compared by incubation of each conjugate in 0.5 M and 0.25 M

NaCl solution. The uncoated AuNPs were clearly destabilised at high salt concentration, which was indicated by the observation of a visible colour change from red to blue. In comparison, pHEA-coated AuNPs remained red in solution at high salt concentrations, due to the steric stabilisation of the nanoparticles, demonstrating their potential for use in physiological media. UV-Vis traces of the AuNPs with saline gradient are shown in (figure 23).

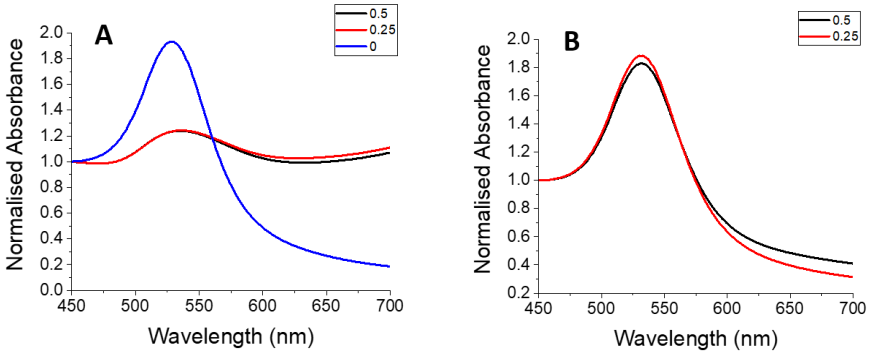

Figure 23: (A) Stability of uncoated AuNPs at 0.5 – 0.25 M NaCl (black, red graphs) compared with 0 M NaCl (blue graph). (B) Stability of polymer-coated AuNPs at 0.5 – 0.25 M NaCl.

3.1.3 Functionalisation of AuNPs with glycans

Glycan-functionalised AuNPs were prepared by the attachment of glycan-polymer conjugates with AuNPs, *via* simple mixing and the excess polymer was removed using centrifugation/resuspension cycles. Lactosamine- and sialyllactosamine-functionalised AuNPs were prepared for implementation in colourimetric detection assays, comparing the difference in aggregation of the glycan-functionalised AuNPs against a panel of different lectins at a range of concentrations.

Lactosamine-functionalised nanoparticles were characterised by UV-Vis and DLS analysis. DLS measurements indicate an increase in NP diameter size upon functionalisation, as expected, from ~50 to ~60 nm. Lactosamine- and sialyllactosamine-AuNP functionalisation was also indicated by a shift in the resonance absorbance peak in the UV-Vis spectrum, from ~528 to 530 nm, indicative of an increase in particle size upon functionalisation (figure 24). TEM imaging showed particles remained well dispersed upon functionalisation (figure 25).

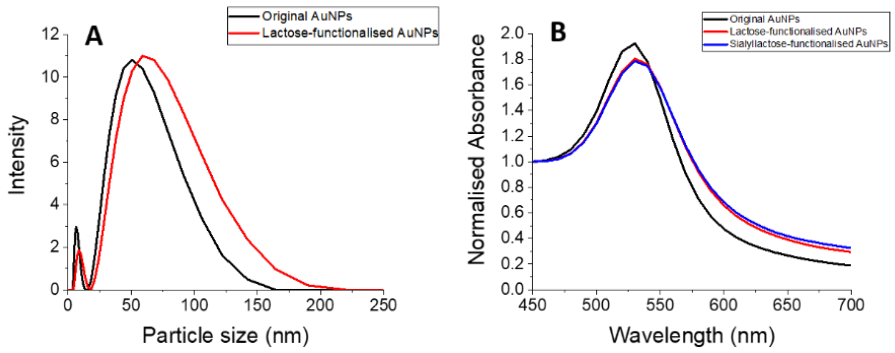

Figure 24: (A) Size difference of functionalised versus unfunctionalised AuNPs as measured by DLS. (B) UV-Vis spectra showing shift in resonance absorbance of functionalised compared with unfunctionalised AuNPs, indicating size difference.

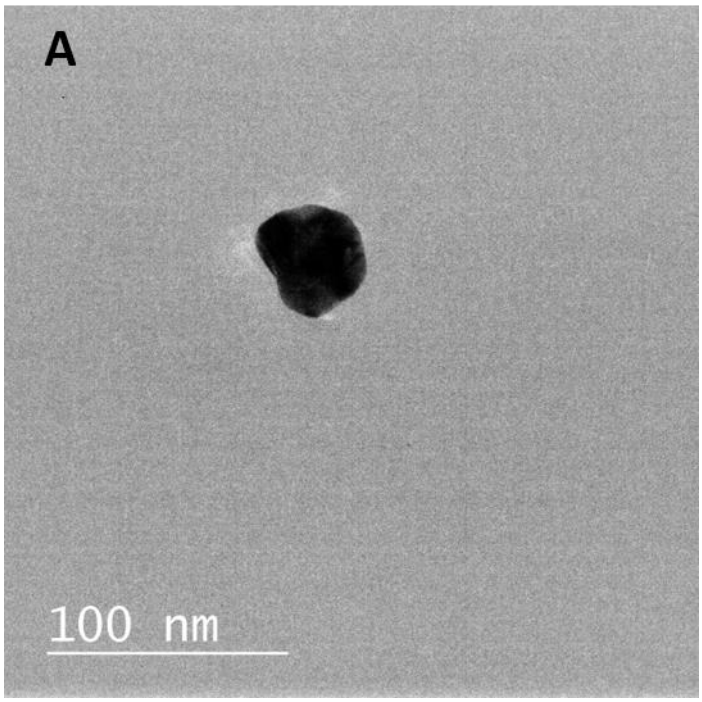

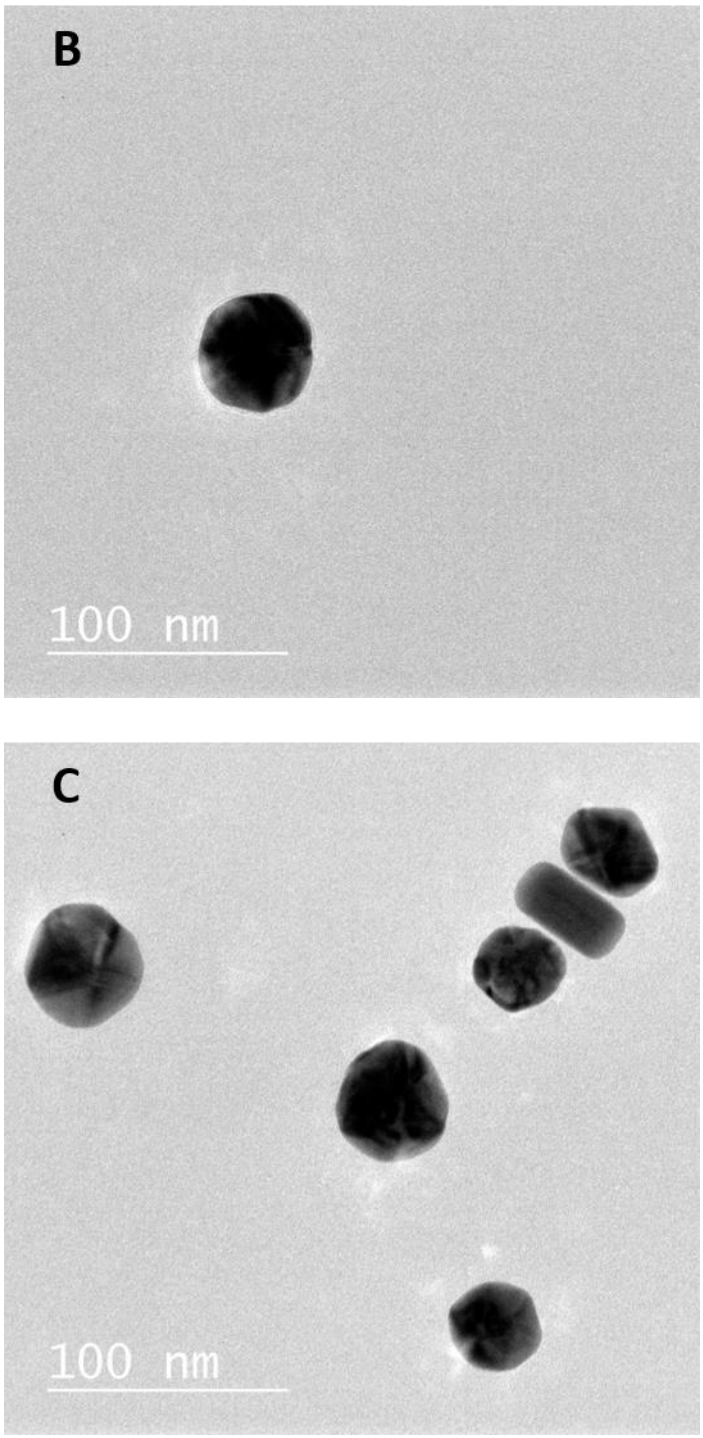

Figure 25: TEM images at 60 000 X magnification of (A) original AuNPs, (B) lactosamine-functionalised AuNPs, (C) sialyllactosamine-functionalised AuNPs.

Table 2: Comparison of functionalised to unfunctionalised gold nanoparticles.

AuNP	**λ_{spr} (nm)**	**Average diameter size by DLS (nm)**
Without functionalisation	528	50
Lactosamine – AuNP conjugate	530	60

3.2 Lectin-induced absorbance aggregation studies

ST enzyme activity is detected in colourimetric sensing assays by monitoring sialic acid transfer from CMP-sialic acid to lactosamine-functionalised AuNPs. Lectin-induced aggregation is compared with lectin-induced aggregation of assays with no enzyme present. A clear difference in binding of lactosamine versus sialylated-AuNPs is expected, based on the affinity of the lectin to each sugar.

AuNP-based colorimetric assays are based on the SPR phenomenon exhibited by the nanoparticles. Resonance absorbance shifts reflect differences in AuNP aggregation, which is initiated by changes in the external environment. Increased AuNP aggregation is characterised by a red shift of the SPR absorbance, accompanied by a solution colour change from red to blue.[32] Lectins were employed as interparticle crosslinking agents, exploiting the multivalent binding of carbohydrates which triggers AuNP aggregation, giving rise to a visually detectable colourimetric readout signifying either positive or negative lectin binding.

GlycoAuNP binding of five different lectins at a range of concentrations was measured in colourimetric detection assays. PNA, RCA and SBA primarily bind to Gal so are expected to aggregate with lactosamine and not with sialyllactosamine. WGA primarily binds to sialic acid, so a more significant binding response is expected with sialyllactosamine. UEA primarily binds Fuc and arabinose so is expected to act as a negative control.

Carbohydrate-lectin binding assays were conducted by the addition of glycosylated AuNPs to a 96-well plate with a dilution series of each lectin in 10 mM HEPES buffer containing 0.05 M NaCl, 0.1 mM $CaCl_2$ and 0.01 mM $MnCl_2$, and incubation of the solution mixtures for 30 minutes. Using a UV-Vis microplate reader, an absorbance spectrum for each sample from 450 nm to 700 nm was obtained.[50] In all the aggregation experiments conducted, the readout at a concentration of 0 lectin can be used as the control to compare shifted absorbance peaks and intensity to the original absorbance peak and intensity.

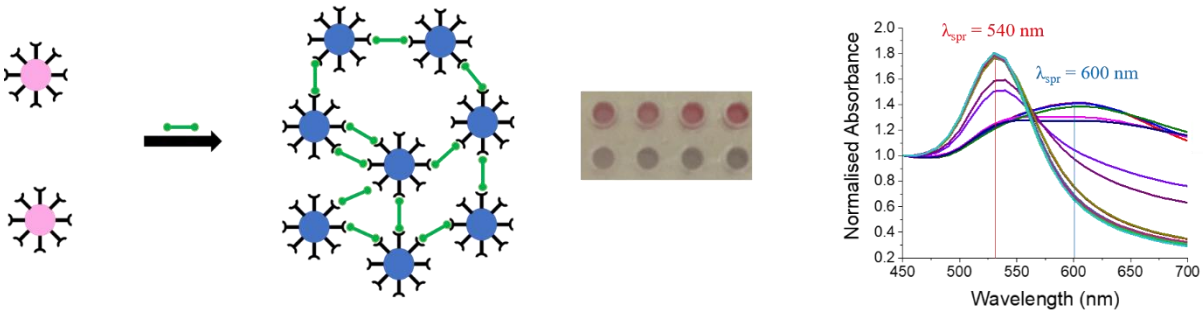

Figure 26: Overview of principle behind absorbance studies. Lectin induced aggregation, indicated by colourimetric detection and a shift in the λ_{spr} signal.

3.2.1 Lectin-induced aggregation without sialyltransferase enzyme

Serial dilutions of PNA, WGA, RCA, SBA and UEA lectins were prepared as detailed above, using an initial lectin concentration of 1 mg.mL^{-1} in the first study and 0.1 mg.mL^{-1} in the second study. Lectin binding assays were constructed using both lactosamine-functionalised AuNPs (figure 27) and sialyllactosamine-functionalised AuNPs (figure 28). AuNPs were used at a concentration of 0.5 mg.mL^{-1}. The resultant absorbance spectra for each assay are shown in Appendices (S1 – S4) and the colourimetric assay results are displayed in figures 27 and 28. AuNP aggregation is characterised in each absorbance spectrum by a decrease in intensity and shift in position of the resonance absorbance peak from ~530 nm to ~600 nm.

The most significant binding response for lactosamine-functionalised AuNPs was clearly exhibited by WGA. Some aggregation also appeared to be observed for RCA and PNA. Sialyllactosamine-functionalised AuNPs in colourimetric assays displayed a clear binding affinity for WGA and a more significant binding response for RCA than was displayed by lactosamine-functionalised AuNPs at a wider range of lectin concentrations.

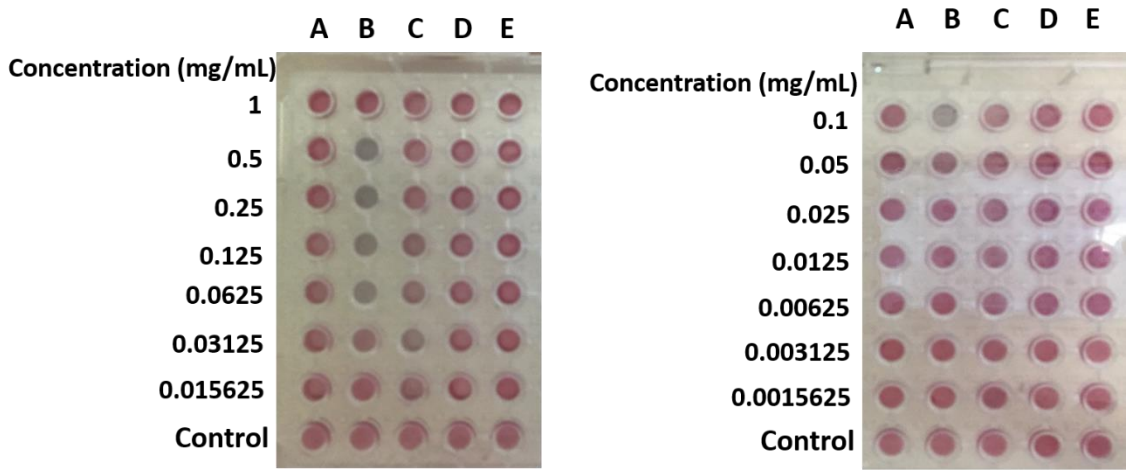

Figure 27: Results from lactosamine-functionalised AuNP assays with (A) PNA, (B) WGA, (C), RCA, (D) SBA and (E) UEA, using an initial lectin concentration of (left) 1 $mg.mL^{-1}$ and (right) 0.1 $mg.mL^{-1}$. A distinctive aggregation response is observed by WGA at a higher lectin concentration.

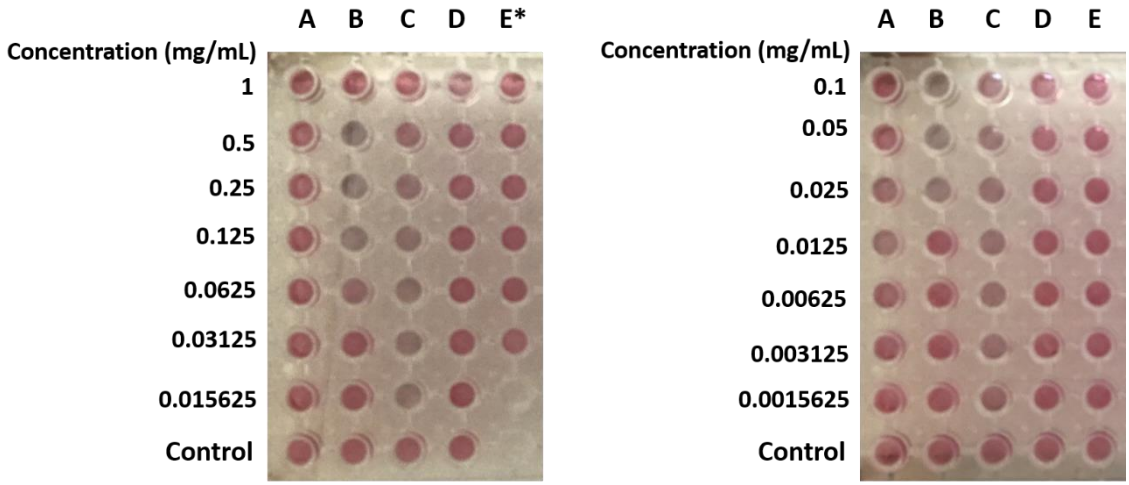

Figure 28: Results from sialyllactosamine-functionalised AuNP assays with (A) PNA, (B) WGA, (C), RCA, (D) SBA and (E) UEA, using an initial lectin concentration of (left) 1 $mg.mL^{-1}$ and (right) 0.1 $mg.mL^{-1}$. A distinctive aggregation response is observed by WGA and by RCA at low lectin concentrations. (**0.015625 mg.mL^{-1} UEA and control UEA results omitted due to sialyllactosamine-AuN solution being finished before these assays were conducted).*

After identification of WGA, RCA and PNA as the lectins which indicated some measure of binding response for lactosamine-functionalised AuNPs, serial dilutions of each of the three lectins were prepared starting from an initial lectin concentration of 0.25 $mg.mL^{-1}$. In the following study conducted, the lectin binding response was monitored as the AuNP concentration was varied between 0.5 $mg.mL^{-1}$ and 0.0625 $mg.mL^{-1}$. The aims of this were to extract the optimum AuNP and lectin concentrations that exhibited a significant

binding response. UV-Vis absorbance spectra for each assay were constructed and the binding isotherms at Abs_{700} were plotted. The results are given in figure 29.

WGA clearly exhibited the optimum binding response, displaying the characteristic sigmoidal-shaped binding curves expected for a positive binding response. The optimum binding response was exhibited at 0.5 $mg.mL^{-1}$ Au. A complete summary of the results identified in these lectin-induced aggregation absorbance assays is given in Table 3.

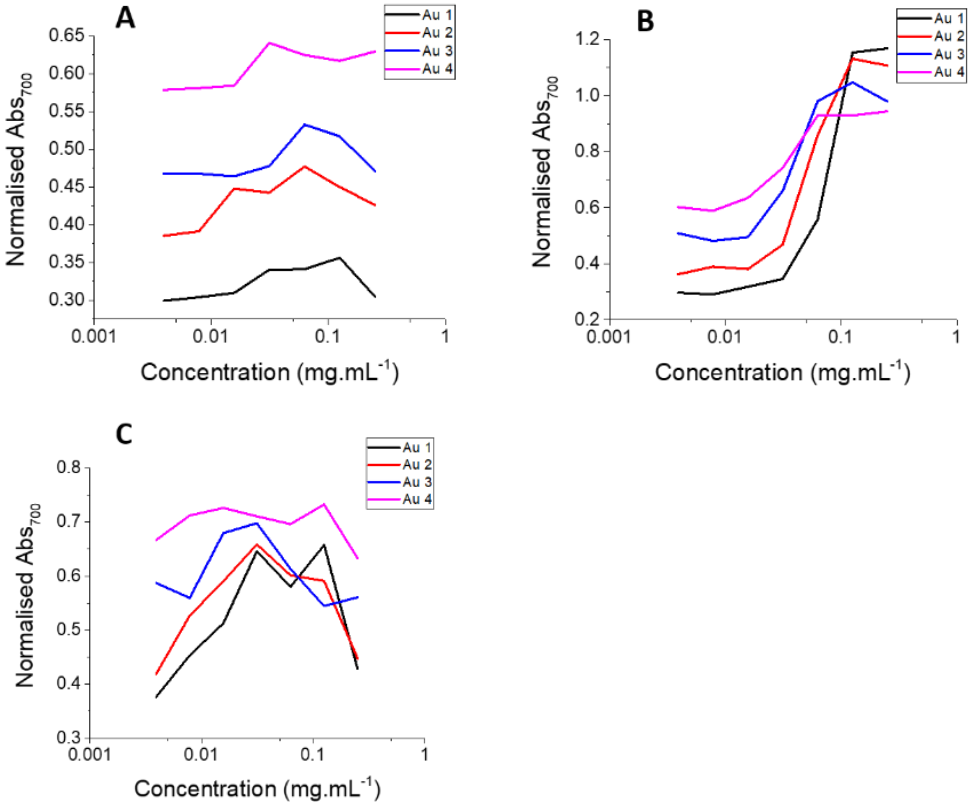

Figure 29: (A) PNA lectin binding at each AuNP concentration. (B) WGA lectin binding at each AuNP concentration. (C) RCA lectin binding at each AuNP concentration. Au 1 = 0.5 $mg.mL^{-1}$, Au 2 = 0.25 $mg.mL^{-1}$, Au 3 = 0.125 $mg.mL^{-1}$, Au 4 = 0.0625 $mg.mL^{-1}$.

Table 3: Summary of aggregation of all lectins with lactosamine and sialyllactosamine.

Lectin	**Sugar specificity**	**Aggregation with lactosamine**	**Aggregation with sialyllactosamine**
PNA	Galactose, sialylation prevents binding	N/A	N/A
WGA	GlcNAc, sialic acid	Significant response at 0.5 – 0.0625 $mg.mL^{-1}$	Significant at 1 – 0.025 $mg.mL^{-1}$
RCA	Galactose, lactose	Some at 0.125 – 0.015625 $mg.mL^{—1}$	Significant at 0.25 – 0.0015625 $mg.mL^{-1}$
SBA	Galactose, GalNAc	N/A	N/A
UEA	Fucose, arabinose	N/A	N/A

3.2.2 Lectin-induced aggregation with sialyltransferase enzyme

The reaction catalysed by α-2,3-sialyltransferase enzyme is detailed in scheme 5. The reaction conditions were optimised using the sugars alone (lactosamine and CMP-sialic acid) before attempting the reaction on particles. To monitor this reaction, enzyme assays were performed (as detailed in section 2.3.6) by incubation of the reaction mixture at 37˚C and allowing the reaction to proceed for 1 – 6 days.

The variables changed were the quantity of enzyme (from 2 µg to 10µg) in the reaction mixture and the length of time of assays incubation (from 1 to 6 days). An aliquot of the reaction mixture was taken for analysis by mass spectroscopy every 24 hours to observe the appearance of the sialyllactosamine product peak (expected mass = 632.2 g mol^{-1}) and disappearance of the reactant peaks (expected mass lactosamine = 341.1 g mol^{-1}, expected mass CMP-sialic acid = 614.2 g mol^{-1}).

The results demonstrated that using 10 µg enzyme and allowing the reaction to proceed for 2 days facilitated optimum enzyme catalysis and yielded a good conversion of lactosamine to sialyllactosamine. These optimum conditions were applied to the proceeding enzymatic assays conducted on particles.

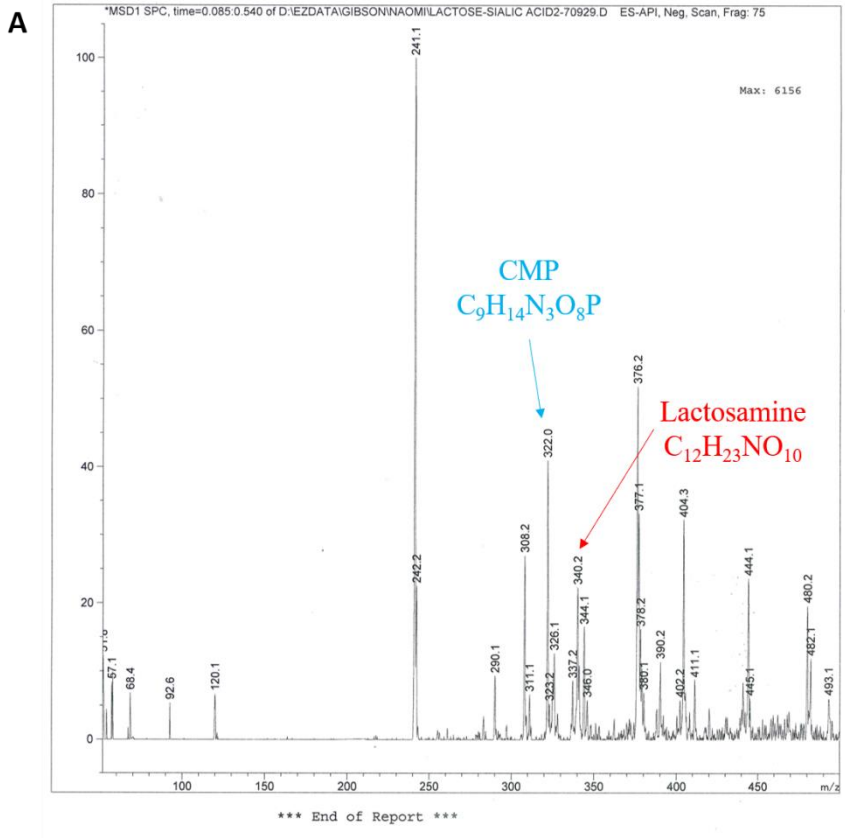

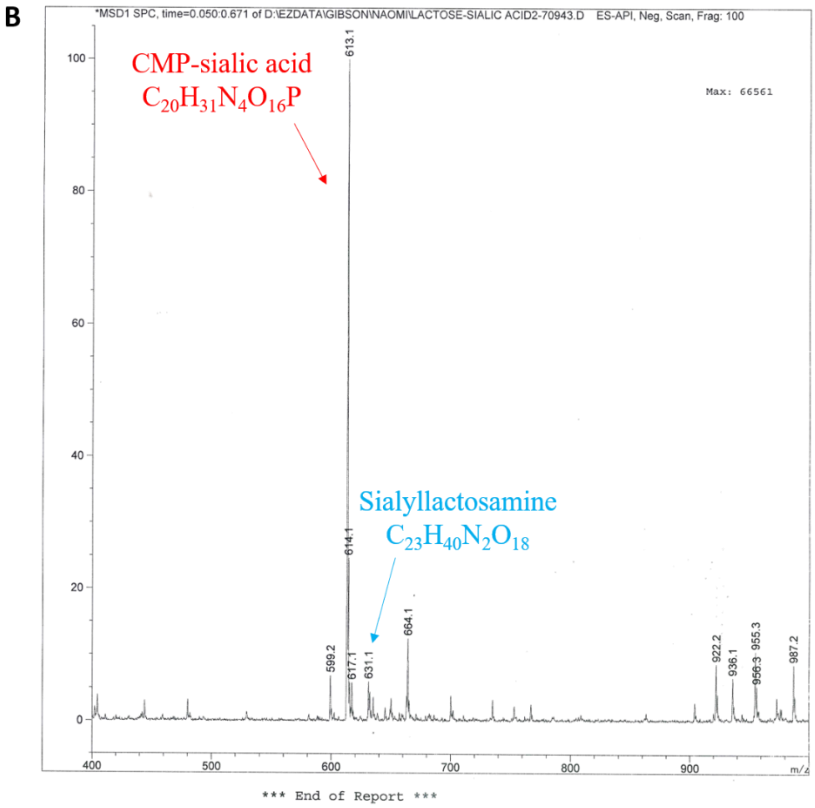

Figure 30: Mass spectrum showing reaction containing mixture of starting material (indicated in red) and products (indicated in blue). (A) CMP and lactosamine molecular ion peaks in the 50 – 500 m/z range. (B) CMP-sialic acid and sialyllactosamine molecular ion peaks in the 400 – 1000 m/z range.

Table 4: Summary of the different reaction conditions applied and the resulting intensity of the sialyllactosamine peak given in the mass spectrum.

Quantity of enzyme	**Incubation time (days)**	**Relative Intensity (%)**	**Ratio intensity Sialyllactosamine : CMP-sialic acid**
2 µg	1	~ 6	1 : 20
4 µg	4	~ 15	1 : 5
10 µg	5	~ 10	1 : 1
10 µg	2	~ 100	20 : 1

Analysis of the reaction progression by mass spectroscopy gave a qualitative indication of which species were present in the reaction mixture. In order to obtain a more quantitative depiction of the species present, an aliquot of the reaction mixture at the optimum conditions was taken for analysis by high performance liquid chromatography (HPLC).

To identify the retention times for lactosamine and sialyllactosamine before quantitative analysis of the reaction mixture, the HPLC column was initially run using prepared standards of lactosamine and sialyllactosamine dissolved in an 80 : 20 acetonitrile : water solution. Using initial column conditions consisting of an 80 : 20 acetonitrile : water eluent and a 2.5 mL/min eluent flow rate, the sugars were found to elute at the same time (table 5). Following this, different column conditions were used to obtain a better sugar separation, but separation was not found to improve as summarised in table 5. This indicated that the sialyllactosamine contained a mixture of lactosamine and sialyllactosamine, giving rise to elution of the product at the retention time observed by lactosamine.

As the optimum column conditions were not identified in this experiment, the reaction mixture aliquot was not analysed by HPLC as this would lead to inconclusive results. Further work needs to be conducted to purify the aminoglycosides before running future columns and to optimise the column conditions required for a good sugar separation.

Table 5: Summary of HPLC conditions attempted and the elution times of the sugars.

Flow rate (mL/min)	**Solvent ratio H_2O : CH_3CN**	**LacNH_2 RI**	**LacNH_2 elution time (min)**	**SialyllacNH_2 RI**	**SialyllacNH_2 elution time (min)**
1	20 : 80	N/A	5.143	N/A	N/A
1 – 2.5	20 : 80	N/A	4.371	N/A	4.371
2.5	20 : 80	2.108	2.005	2.142	1.929
2.5	40 : 60	2.811	2.156	2.797	2.158

Enzymatic lectin-induced aggregation absorbance assays were conducted using 10 μg sialyltransferase enzyme, sugar-functionalised AuNPs at 0.5 $mg.mL^{-1}$ Au and varying the concentrations of WGA and RCA lectin between 0.125 – 0.5 $mg.mL^{-1}$. Results were compared to lactosamine-functionalised and sialyllactosamine-functionalised AuNPs without enzyme present as a control (figures 31 and 32).

There was a clear difference observed between the binding response seen with the control lactosamine-functionalised AuNPs and the enzyme-assayed AuNPs, which indicates that some sialic acid transfer to the AuNPs took place and was detected by a change in binding response. Despite this, the results obtained did not precisely fit the binding response observed by the lectins with control sialyllactosamine-functionalised AuNPs, which could indicate that the amount of sialic acid transferred to the glycoAuNPs was not a high enough concentration to cause significant lectin binding.

It should be noted that sialyllactosamine-functionalised and lactosamine-functionalised control experimental results were also compared with previous sialyllactosamine-AuNP and lactosamine-AuNP results (figures 27 and 28) and that there was a clear difference observed in these experiments. Considerably less aggregation was observed for the control experiments for both WGA and RCA in comparison to the previous results obtained. In particular, the sialyllactosamine binding response with RCA was considerably less distinctive in the control experiment conducted as compared with previous experimental results. This could indicate that the lectins were not functioning as well, potentially due to dilution solutions having been previously prepared and stored in the freezer until needed, hence binding to the sugars was not as effective as previous experimental results had indicated, or due to insufficient conversion of lactosamine to sialyllactosamine to cause aggregation.

Ultimately, the change in binding response observed between enzymatic-assayed AuNPs and control lactosamine-functionalised AuNPs serves as a good initial indication that some sialic acid transfer took place but is limited in indicating if there was a significant amount of sialic acid transfer due to limited function of the lectins used in this assay. Essentially, this provides a good scope for further experimental work to develop and refine this assay technique.

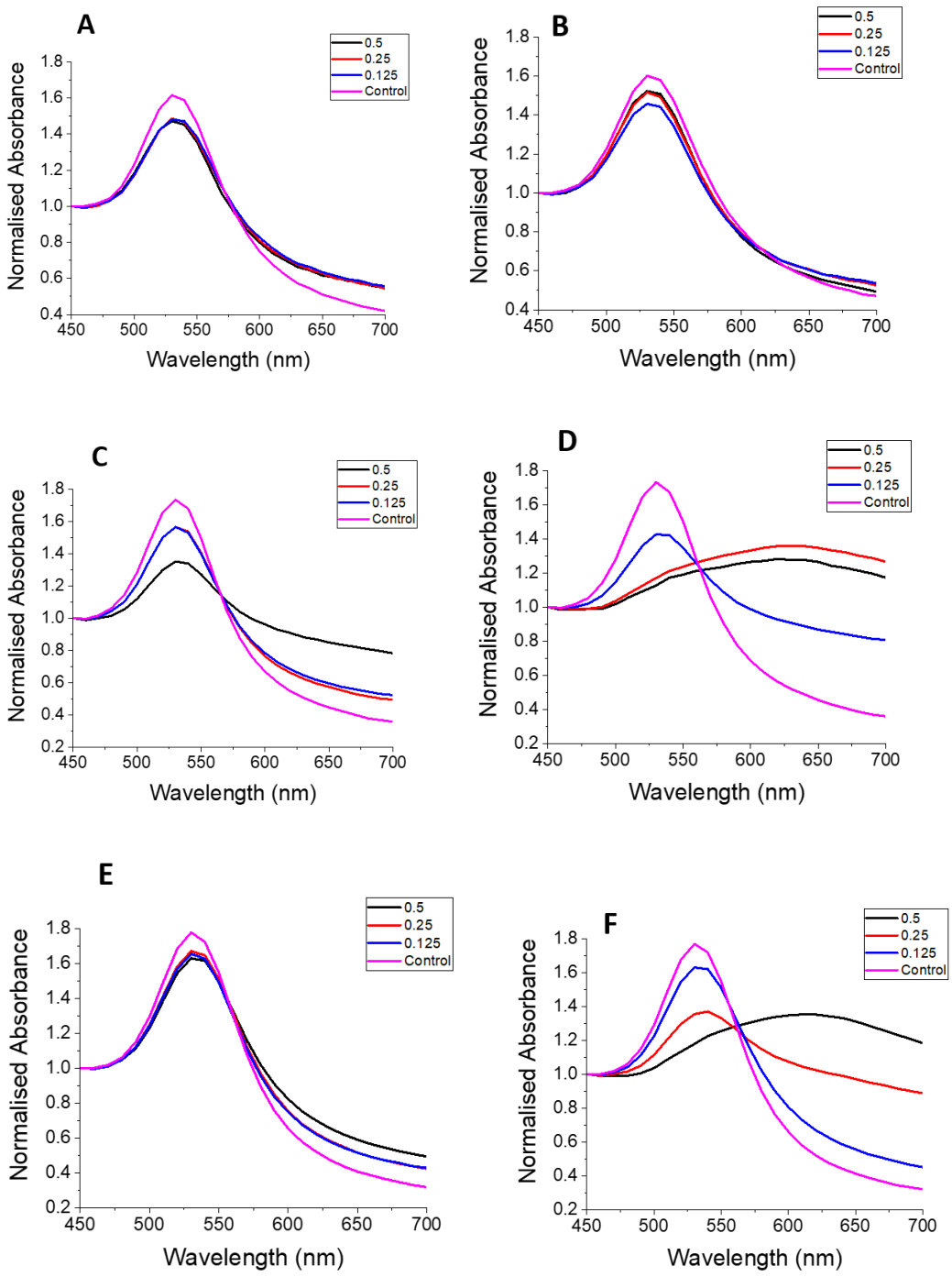

Figure 31: (A) and (B) are the resultant UV-Vis absorbance spectra from enzymatic assay studies. (C), (D), (E) and (F) are control results from aggregation studies without enzyme present. (A) Enzymatic assay with RCA, (B) Enzymatic assay with WGA, (C) Lactosamine-functionalised AuNPs with RCA, (D) Lactosamine-functionalised AuNPs with WGA, (E) Sialyllactosamine-functionalised AuNPs with RCA, (F) Sialyllactosamine-functionalised AuNPs with WGA.

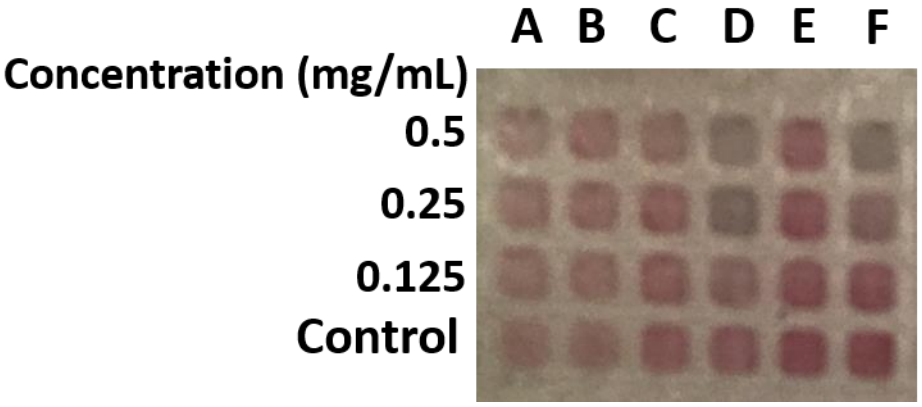

Figure 32: Colourimetric depiction of assay results.

4 Conclusions and Future Work

A simplistic colourimetric sensing method utilising glycan-functionalised AuNPs was established for detection of ST enzyme activity. The results gained from this study show much potential for the development of a sensitive and simple assay tool to be employed for target compound screening.

Glycan-functionalised AuNPs were prepared using a well-refined, tuneable approach that facilitated production of stabilised AuNPs of desired size. The stabilising polymer coating applied improved NP stability whilst maintaining high sensitivity of the nanoparticles on implementation of the NPs in colourimetric assays. Conjugation of the NPs with aminoglycosides was conducted *via* initial glycosylation of the polymer, before application to the NP surface. This approach ensured full characterisation of the polymer-sugar conjugate prior to surface modification.

Glyconanoparticle conjugates were successfully employed in colourimetric detection assays in which aggregation was induced by incubation of nanoparticles with lectins. Despite noting a difference in observed lectin binding compared with expected lectin binding, a notable difference in binding was observed between lactosamine-functionalised NPs, compared with sialyllactosamine-functionalised NPs, highlighting the sensitivity of the colourimetric detection system. In this study, a greater range of concentrations of RCA demonstrated a much higher binding affinity to sialyllactosamine, and lower concentrations of WGA demonstrated a higher binding specificity to lactosamine.

Additionally, reaction parameters for α-2,3-sialyltransferase enzymatic assays were optimised enabling good qualitative conversion of starting material to the product. A quantitative representation of conversion can be extracted using HPLC analysis, which requires continued optimisation of the HPLC column conditions to obtain a good separation between sugars. Alternatively, sialic acid functionalisation could be determined by X-ray photoelectron spectroscopy (XPS) measurements. Once reaction conversion has been identified, this will also give an indication of any further refinements which could be applied to enzymatic assay conditions.

Whilst implementation of glyconanoparticles in colourimetric detection assays of sialyltransferase enzyme did not precisely match results for sialyllactosamine-functionalised AuNPs, the results obtained still demonstrated a distinctive difference in both WGA and RCA lectin binding response in comparison to lactosamine-functionalised

AuNPs which were used as a control. The observed binding responses were limited due to possible decrease in functionality of the WGA and RCA lectins employed in these assays, as there was a decrease in the measured control binding responses compared with previous assay results. Replication of these experiments will provide a consistent and reliable set of results for comparison and accurate determination of which lectins give rise to the most significant binding responses and at which concentrations.

Ultimately, a sensitive assay tool was developed that was able to show a difference in lectin binding upon enzyme action. This technique shows much potential for further work to be conducted, including screening of different lectins which could display an even more prominent difference in binding affinity between lactosamine and sialyllactosamine than was demonstrated by WGA and RCA. Other future work could be to use more relevant enzymes such as α-2,6-sialyltransferase which has been possibly linked to β-secretase enzyme activity.[3]

Indeed, this work could be used as a basis for the development of simple, low-cost biosensors to be applied for the detection of abnormal sialylation in AD. In this case, the glycosylated-AuNPs colourimetric assay sensing system would be applied as an investigative tool to detect differences in sialyltransferase enzyme activity. In order to conduct this work, the establishment of a replicable assay that has demonstrated accurate and consistent experimental results is critical. Additionally, ensuring that AuNP stability is maintained is essential for translation of the detection system into biological systems. A potential sensitive, AuNP-based colourimetric biosensing system has been established by this work, which provides a good foundation to be further built upon.

5 References

1 C. Reitz and R. Mayeux, *Biochem. Pharmacol.*, 2014, **88**, 640–651.

2 Y. Miura and T. Endo, *Biochim. Biophys. Acta - Gen. Subj.*, 2016, **1860**, 1608–1614.

3 S. Schedin-Weiss, B. Winblad and L. O. Tjernberg, *FEBS J.*, 2014, **281**, 46–62.

4 K. Kanninen, G. Goldsteins, S. Auriola, I. Alafuzoff and J. Koistinaho, *Neurosci. Lett.*, 2004, **367**, 235–240.

5 L. R. Fodero, J. Sáez-Valero, M. S. Barquero, A. Marcos, C. A. McLean and D. H. Small, *J. Neurochem.*, 2001, **79**, 1022–1026.

6 D. S. Yang, A. Tandon, F. Chen, G. Yu, H. Yu, S. Arawaka, H. Hasegawa, M. Duthie, S. D. Schmidt, T. V. Ramabhadran, R. A. Nixon, P. M. Mathews, S. E. Gandy, H. T. J. Mount, P. S. George-Hyslop and P. E. Fraser, *J. Biol. Chem.*, 2002, **277**, 28135–28142.

7 J. Charlwood, C. Dingwall, R. Matico, I. Hussain, K. Johanson, S. Moore, D. J. Powell, J. M. Skehel, S. Ratcliffe, B. Clarke, J. Trill, S. Sweitzer and P. Camilleri, *J. Biol. Chem.*, 2001, **276**, 16739–16748.

8 Y. Kizuka, S. Kitazume and N. Taniguchi, *Biochim. Biophys. Acta - Gen. Subj.*, 2017, **1861**, 2447–2454.

9 T. Dunckley, K. D. Coon and D. A. Stephan, *Drug Discov. Today*, 2005, **10**, 326–334.

10 H. Seitz, *Molecular Diagnostics*, 2014, vol. 52.

11 N. Mattsson, *Clin. Chem. Lab. Med.*, 2011, **49**, 345–352.

12 A. Palmigiano, R. Barone, L. Sturiale, C. Sanfilippo, R. O. Bua, D. A. Romeo, A. Messina, M. L. Capuana, T. Maci, F. Le Pira, M. Zappia and D. Garozzo, *J. Proteomics*, 2016, **131**, 29–37.

13 N. Xia, L. Liu, M. G. Harrington, J. Wang and F. Zhou, *Anal. Chem.*, 2010, **82**, 10151–10157.

14 D. R. Thevenot, *Pure Appl. Chem.*, 1999, **71**, 2333–2348.

15 K. Saha, S. S. Agasti, C. Kim, X. Li and V. M. Rotello, *Chem. Rev.*, 2012, **112**, 2739–2779.

16 P. Bertoncello and R. J. Forster, *Biosens. Bioelectron.*, 2009, **24**, 3191–3200.

17 F.-W. Bai, C.-G. Liu, H. Huang and G. T. Tsao, *Advances in Biochemical Engineering / Biotechnology*, 2012.

18 X. Jia, X. Xu and L. Zhang, *Biomacromolecules*, 2013, **14**, 1787–1794.

19 S. Watanabe, K. Yoshida, K. Shinkawa, D. Kumagawa and H. Seguchi, *Colloids Surfaces B Biointerfaces*, 2010, **81**, 570–577.

20 L. A. Dykman and N. G. Khlebtsov, *Acta Naturae*, 2011, **3**, 34–55.

21 J. E. Ghadiali and M. M. Stevens, *Adv. Mater.*, 2008, **20**, 4359–4363.

22 P. C. H. J. Turkevich, J; Stevenson, *Discuss. Faraday Soc.*, 1951, **11**, 55–75.

23 N. G. Bastús, J. Comenge and V. Puntes, *Langmuir*, 2011, **27**, 11098–11105.

24 N. Sze Ieong, C. I. Biggs, M. Walker and M. I. Gibson, *J. Polym. Sci. Part A Polym. Chem.*, 2017, **55**, 1200–1208.

25 R. Subbiah, M. Veerapandian and K. . Yun, *Curr. Med. Chem.*, 2010, **17**, 4559–4577.

26 M.-A. Neouze and U. Schubert, *Monatshefte für Chemie - Chem. Mon.*, 2008, **139**, 183–195.

27 A. P. Philipse, A. M. Nechifor and C. Patmamanoharan, *Langmuir*, 1994, **10**, 4451–4458.

28 L. Otten, D. Vlachou, S.-J. Richards and M. I. Gibson, *Analyst*, 2016, **141**, 4305–4312.

29 W. Rechberger, A. Hohenau, A. Leitner, J. R. Krenn, B. Lamprecht and F. R. Aussenegg, *Opt. Commun.*, 2003, **220**, 137–141.

30 S. Zeng, D. Baillargeat, H.-P. Ho and K.-T. Yong, *Chem. Soc. Rev.*, 2014, **43**, 3426.

31 P. K. Jain, K. S. Lee, I. H. El-Sayed and M. A. El-Sayed, *J. Phys. Chem. B*, 2006, **110**, 7238–7248.

32 H. Aldewachi, T. Chalati, M. N. Woodroofe, N. Bricklebank, B. Sharrack and P. H. Gardiner, *Nanoscale*, 2017, 18–33.

33 J. H. Soh, Y. Lin, S. Rana, J. Y. Ying and M. M. Stevens, *Anal. Chem.*, 2015, **87**, 7644–7652.

34 M. J. Marín, C. L. Schofield, R. A. Field and D. A. Russell, *Analyst*, 2015, **140**, 59–70.

35 J. Liu and Y. Lu, *Adv. Mater.*, 2006, **18**, 1667–1671.

36 J. Liu, D. Mazumdar and Y. Lu, *Angew. Chemie - Int. Ed.*, 2006, **45**, 7955–7959.

37 A. Talib, M. S. Khan, G. R. Gedda and H. F. Wu, *J. Mol. Liq.*, 2016, **220**, 463–467.

38 K. Matyjaszewski and J. Spanswick, *Mater. Today*, 2005, **8**, 26–33.

39 S. Perrier and P. Takolpuckdee, *J. Polym. Sci. Part A Polym. Chem.*, 2005, **43**, 5347–5393.

40 J. Conde, J. T. Dias, V. Grazú, M. Moros, P. V. Baptista and J. M. de la Fuente, *Front. Chem.*, 2014, **2**, 1–27.

41 R. Rojanathanes, A. Sereemaspun, N. Pimpha, V. Buasorn, P. Ekawong and V. Wiwanitkit, *Taiwan. J. Obstet. Gynecol.*, 2008, **47**, 296–299.

42 P. Eaton, G. Doria, E. Pereira, P. V. Baptista and R. Franco, *IEEE Trans. Nanobioscience*, 2007, **6**, 282–288.

43 J. S. Lee, P. A. Ulmann, M. S. Han and C. A. Mirkin, *Nano Lett.*, 2008, **8**, 529–533.

44 R. A. Reynolds, C. A. Mirkin and R. L. Letsinger, *J. Am. Chem. Soc.*, 2000, **122**, 3795–3796.

45 X. Xu, W. L. Daniel, W. Wei and C. A. Mirkin, *Small*, 2010, **6**, 623–626.

46 S. Huang, Q. Xiao, R. Li, H. L. Guan, J. Liu, X. R. Liu, Z. K. He and Y. Liu, *Anal. Chim. Acta*, 2009, **645**, 73–78.

47 S. Wu, X. Lan, F. Huang, Z. Luo, H. Ju, C. Meng and C. Duan, *Biosens. Bioelectron.*, 2012, **32**, 293–296.

48 C. D. Medley, J. E. Smith, Z. Tang, Y. Wu, S. Bamrungsap and W. Tan, *Anal. Chem.*, 2008, **80**, 1067–1072.

49 S. J. Richards and M. I. Gibson, *ACS Macro Lett.*, 2014, **3**, 1004–1008.

50 S.-J. Richards, L. Otten and M. I. Gibson, *J. Mater. Chem. B*, 2016, **4**, 3046–3053.

51 J. J. Lundquist and E. J. Toone, *Chem. Rev.*, 2002, **102**, 555–578.

52 S. M. Dimick, S. C. Powell, S. A. McMahon, D. N. Moothoo, J. H. Naismith and E. J. Toone, *J. Am. Chem. Soc.*, 1999, **121**, 10286–10296.

53 D. J. Phillips and M. I. Gibson, *Biomacromolecules*, 2012, **13**, 3200–3208.

54 W. Haiss, N. T. K. Thanh, J. Aveyard and D. G. Fernig, 2015, **79**, 4215–4221.

55 S.-J. Richards, E. Fullam, G. S. Besra and M. I. Gibson, *J. Mater. Chem. B*, 2014, **2**, 1490–1498.

56 V. S. Godakhindi, P. Kang, M. Serre, N. A. Revuru, J. M. Zou, M. R. Roner, R. Levitz, J. S. Kahn, J. Randrianalisoa and Z. Qin, *ACS Sensors*, 2017, **2**, 1627–1636.

6 Appendices

6.1 Results of lectin-induced aggregation absorbance studies with lactosamine-functionalised AuNPs

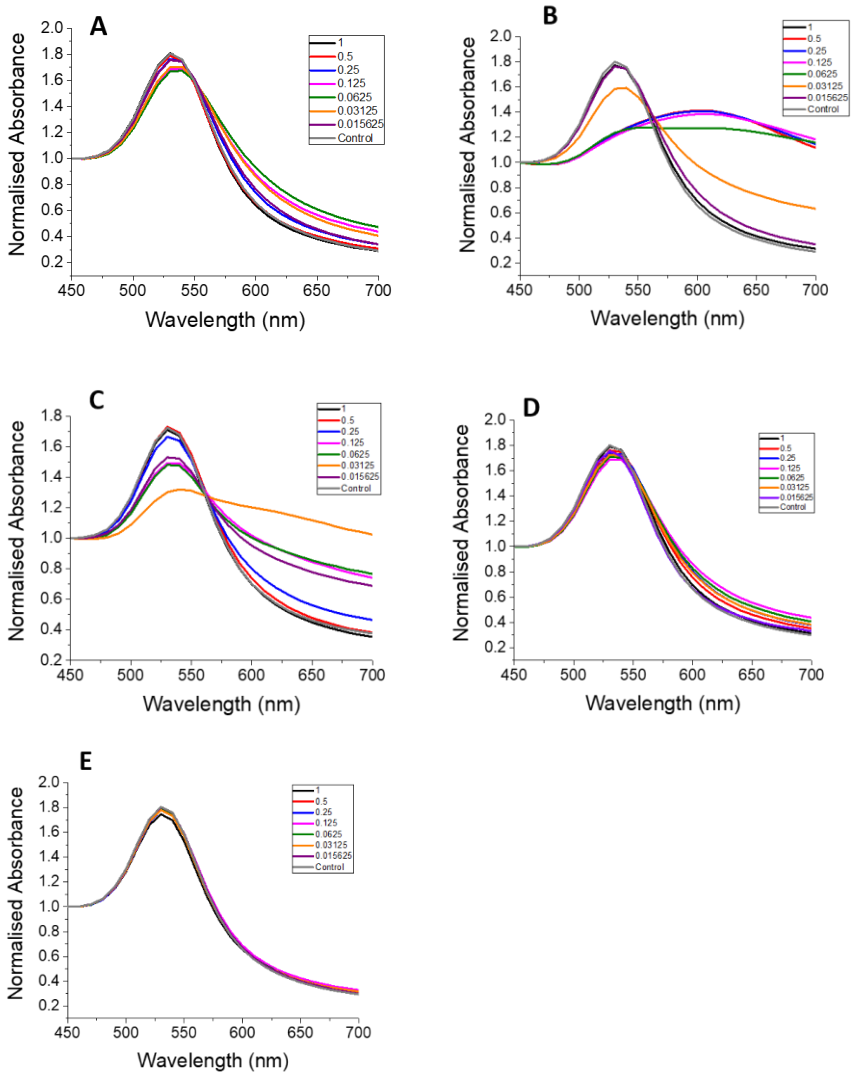

Figure S1: Results from lactosamine-functionalised AuNPs aggregation with (A) PNA, (B) WGA, (C) RCA, (D) SBA and (E) UEA, using an initial lectin concentration of 1 $mg.mL^{-1}$.

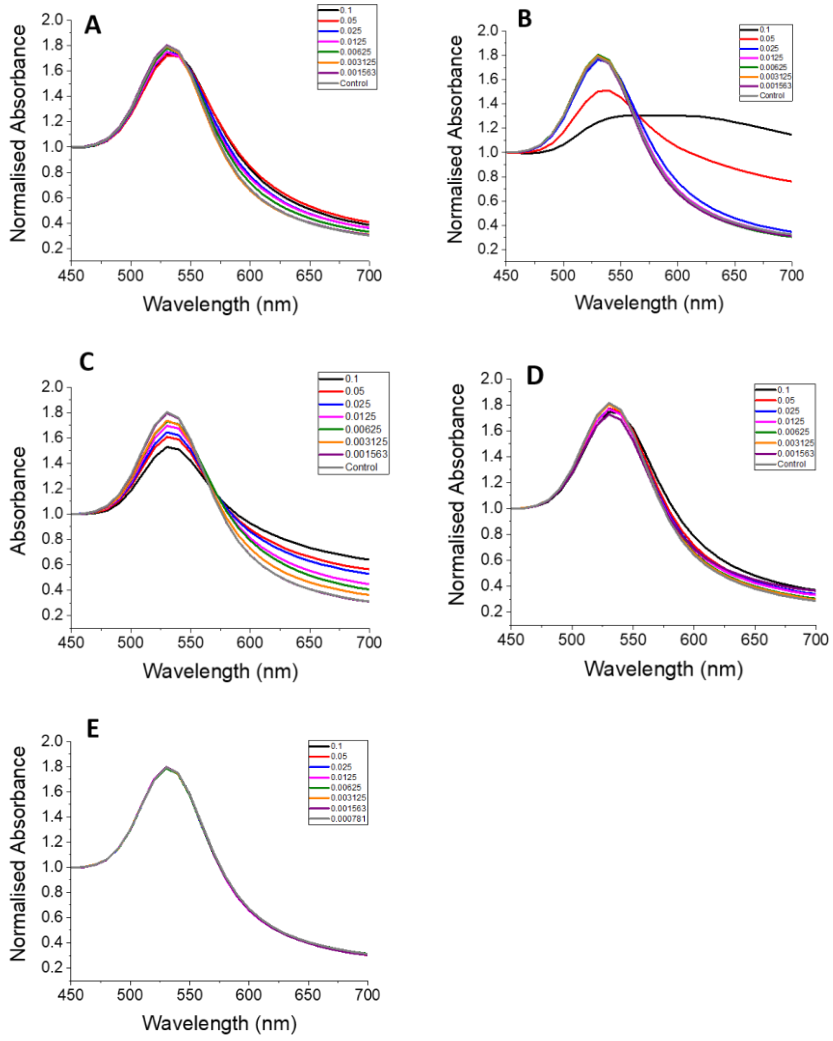

Figure S2: Results from lactosamine-functionalised AuNPs aggregation with (A) PNA, (B) WGA, (C) RCA, (D) SBA and (E) UEA, using an initial lectin concentration of 0.1 $mg.mL^{-1}$.

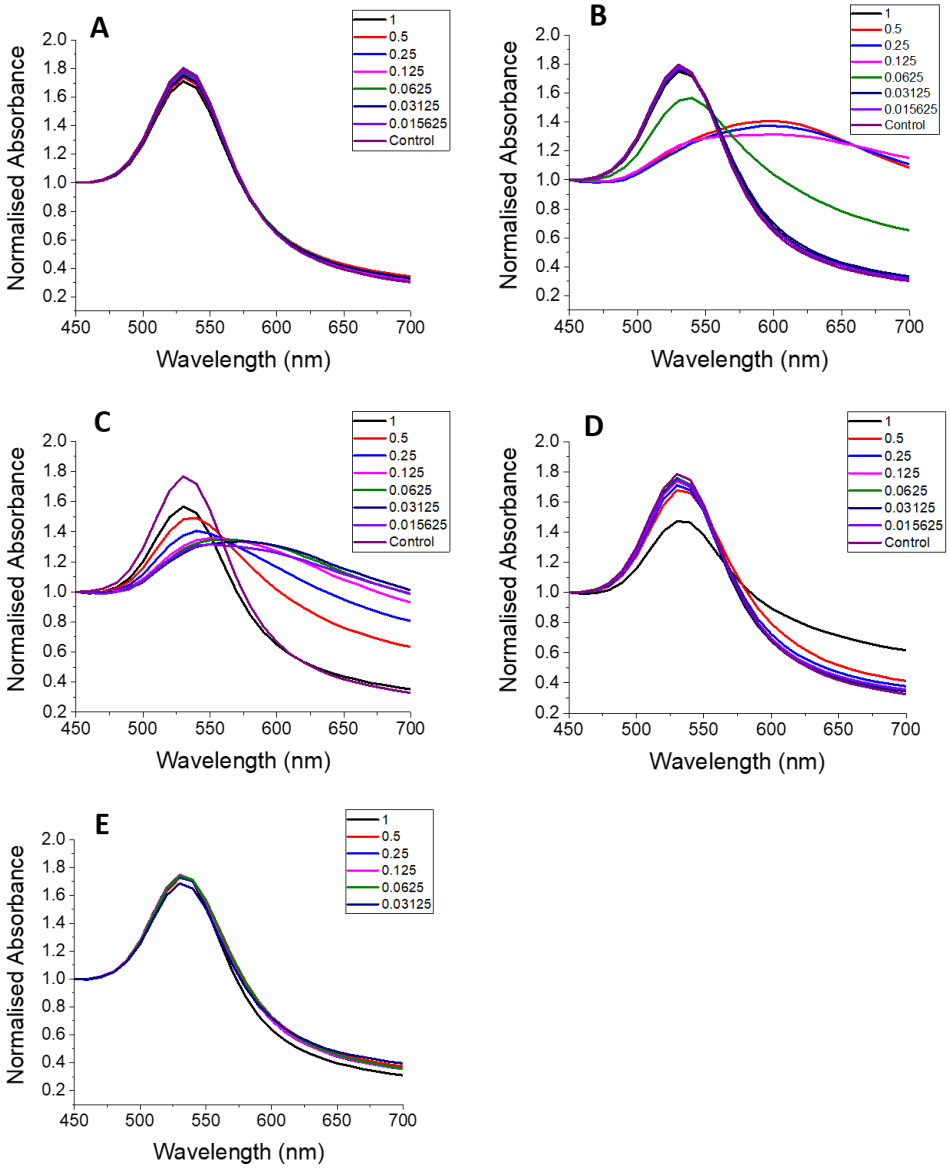

Figure S3: Results from sialyllactosamine-functionalised AuNPs aggregation with (A) PNA, (B) WGA, (C) RCA, (D) SBA and (E) UEA, using an initial lectin concentration of 1 $mg.mL^{-1}$.

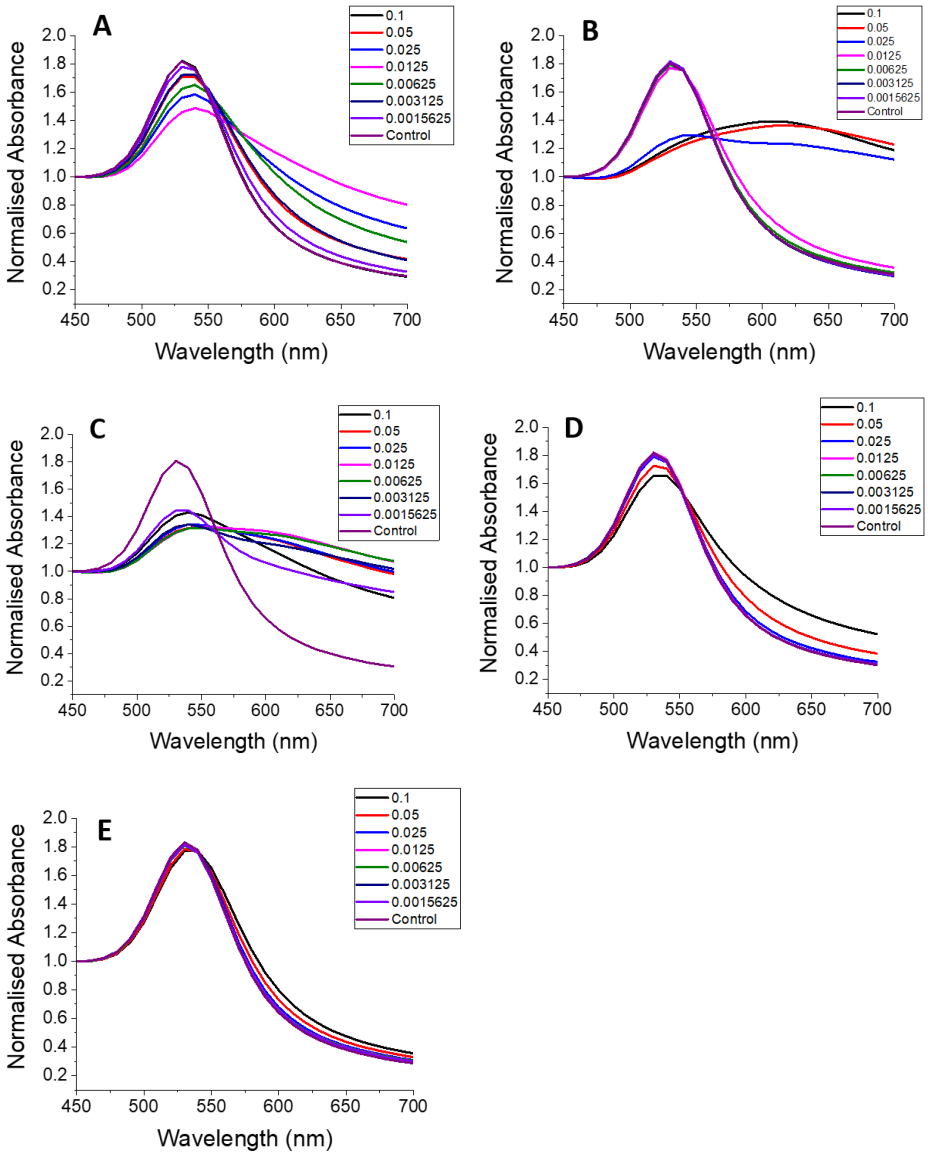

Figure S4: Results from sialyllactosamine-functionalised AuNPs aggregation with (A) PNA, (B) WGA, (C) RCA, (D) SBA and (E) UEA, using an initial lectin concentration of 0.1 mg.mL^{-1}.

6.2 HPLC trace of lactosamine and sialyllactosamine at different column conditions

For all except indicated the solvent conditions used were 20 : 80 H_2O : CH_3CN.

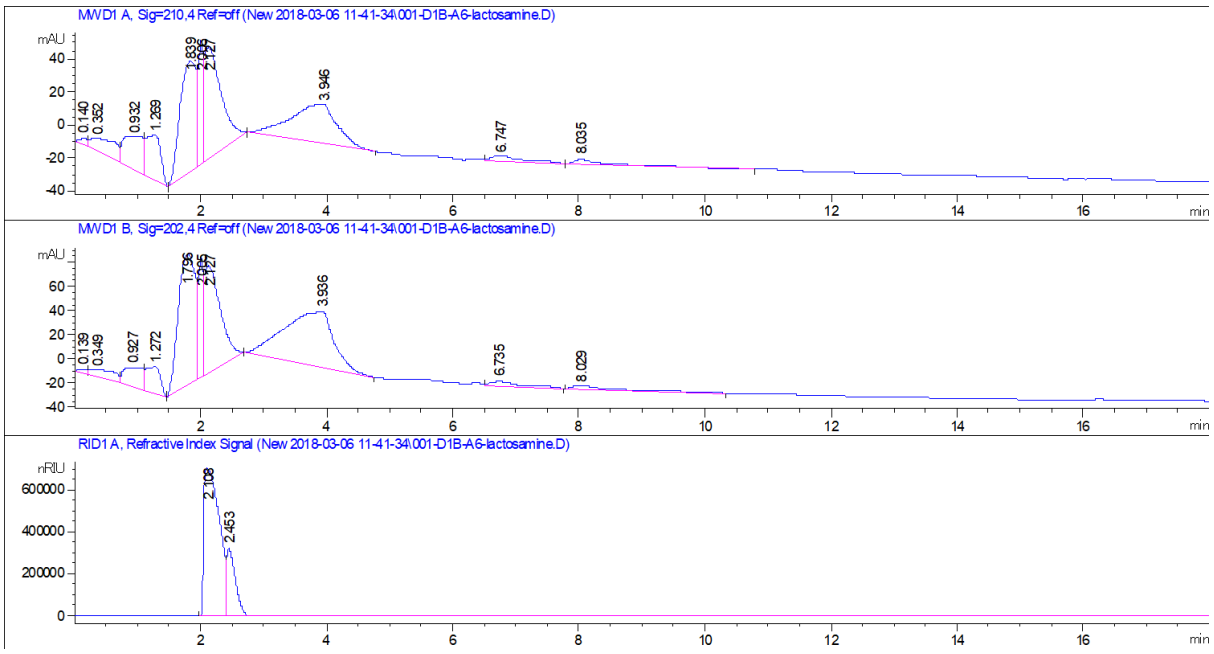

Figure S5: HPLC trace lactosamine. 2.5 mL/min flow rate. Elution time 2.005 min.

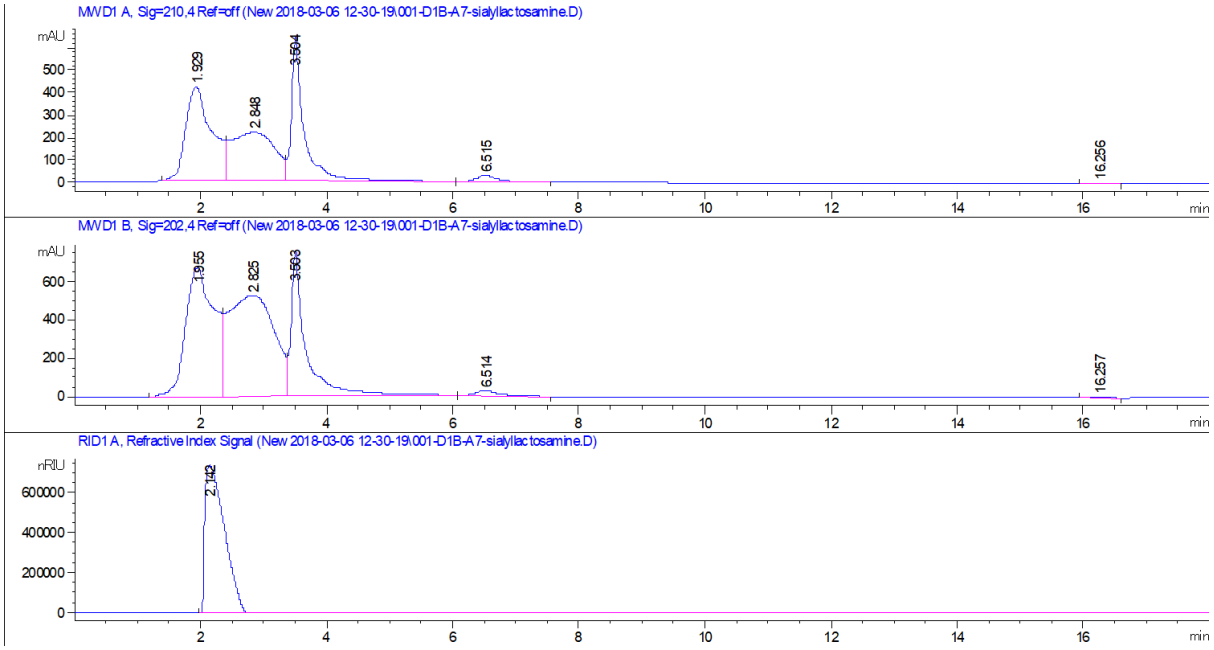

Figure S6: HPLC trace sialyllactosamine. 2.5 mL/min flow rate. Elution time 1.929 min.

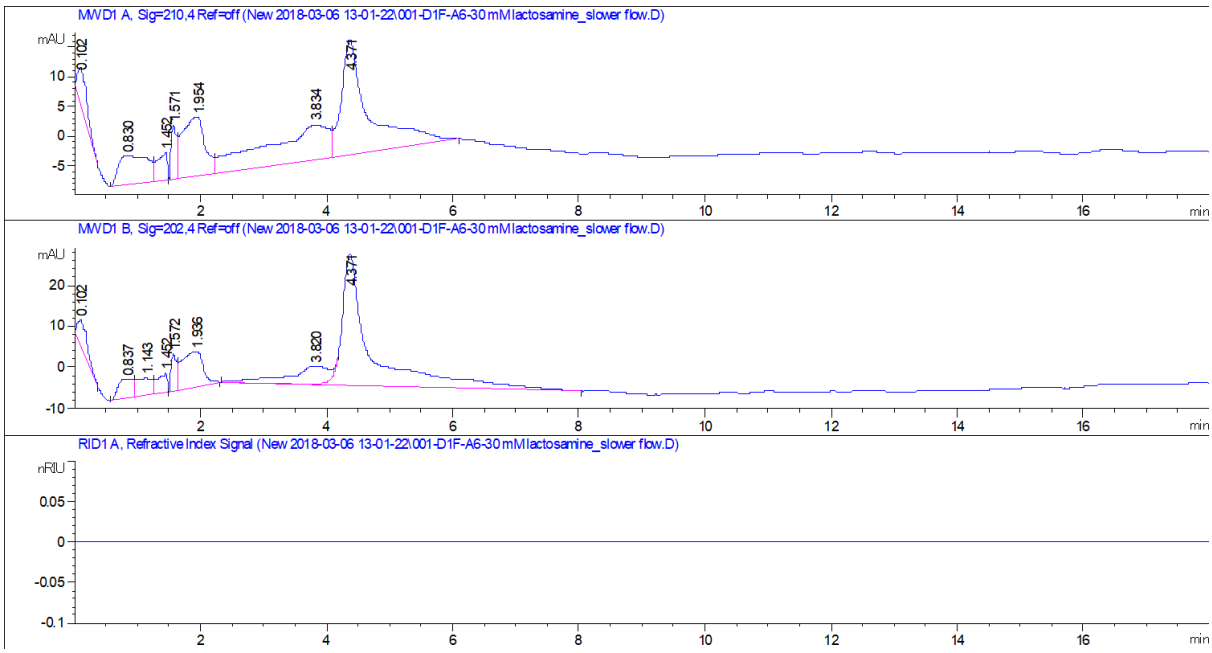

Figure S7: HPLC trace lactosamine. 1 – 2.5 mL/min flow rate. Elution time 4.371 min.

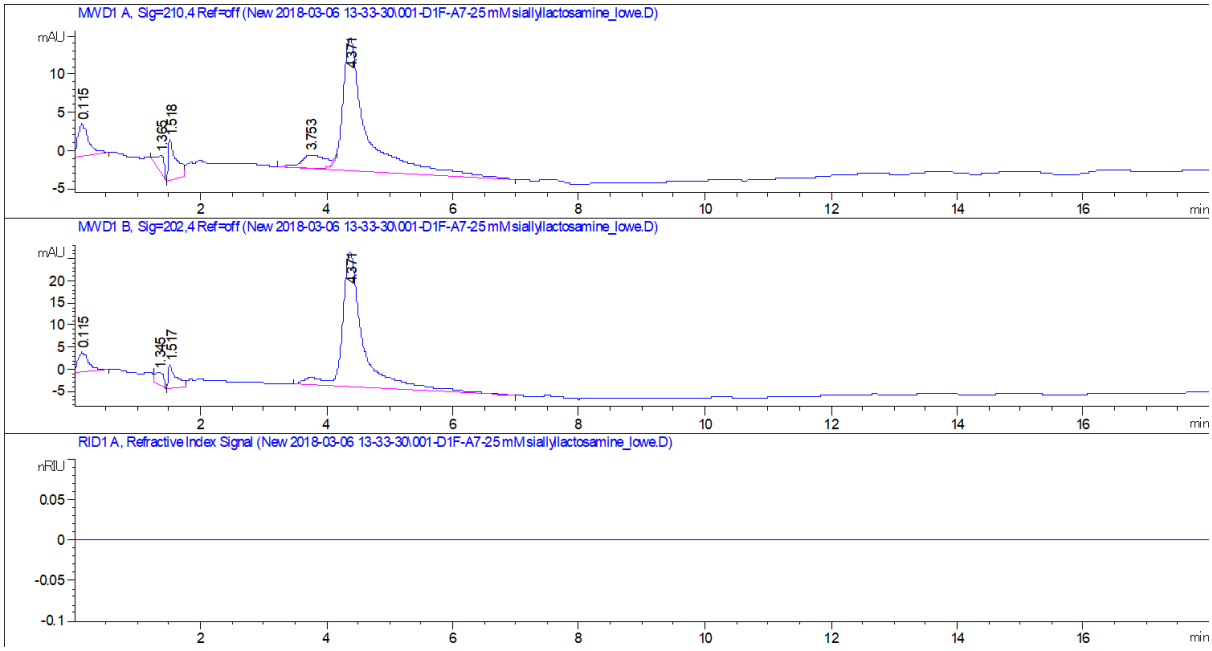

Figure S8: HPLC trace sialyllactosamine. 1 – 2.5 mL/min flow rate. Elution time 4.371 min.

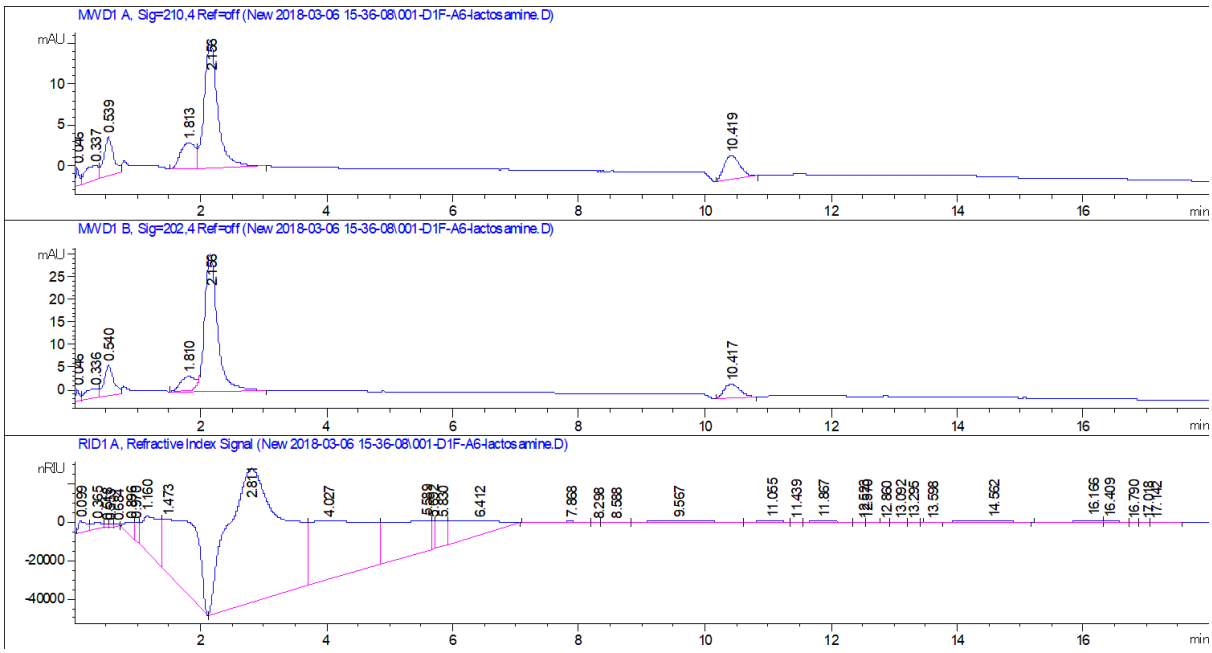

Figure S9: HPLC trace lactosamine. Solvent ratio 40 : 60 H_2O : CH_3CN. 2.5 mL/min flow rate. Elution time 2.156 min.

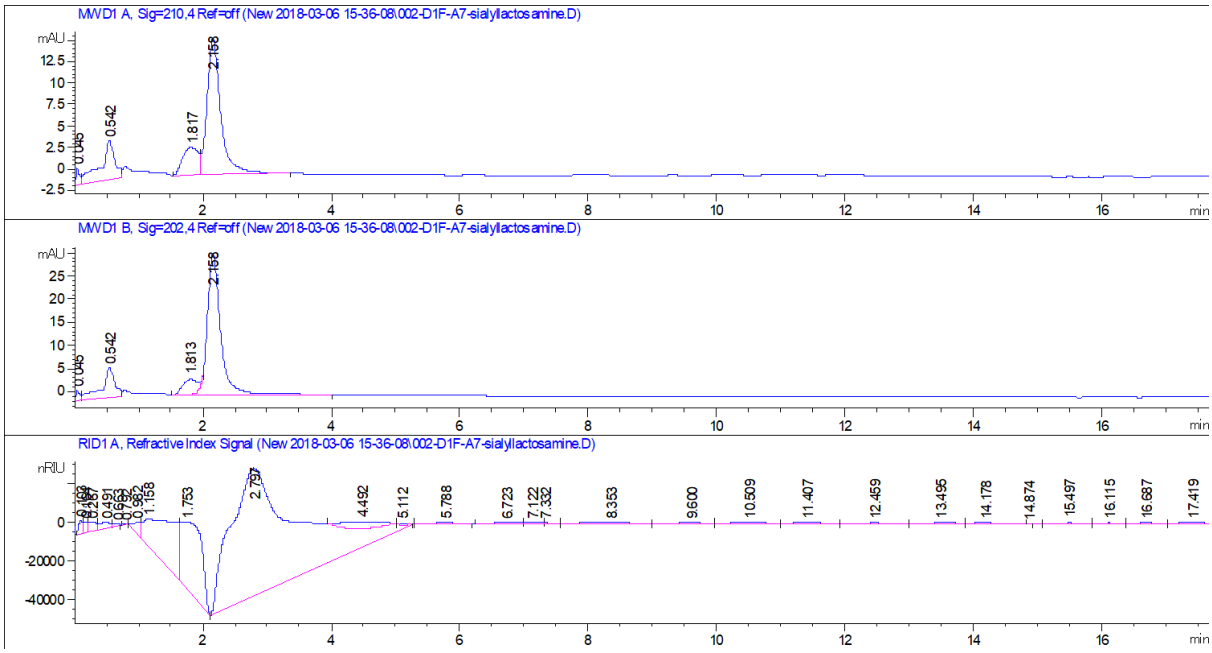

Figure S10: HPLC trace sialyllactosamine. Solvent ratio 40 : 60 H_2O : CH_3CN. 2.5 mL/min flow rate. Elution time 2.158 min.

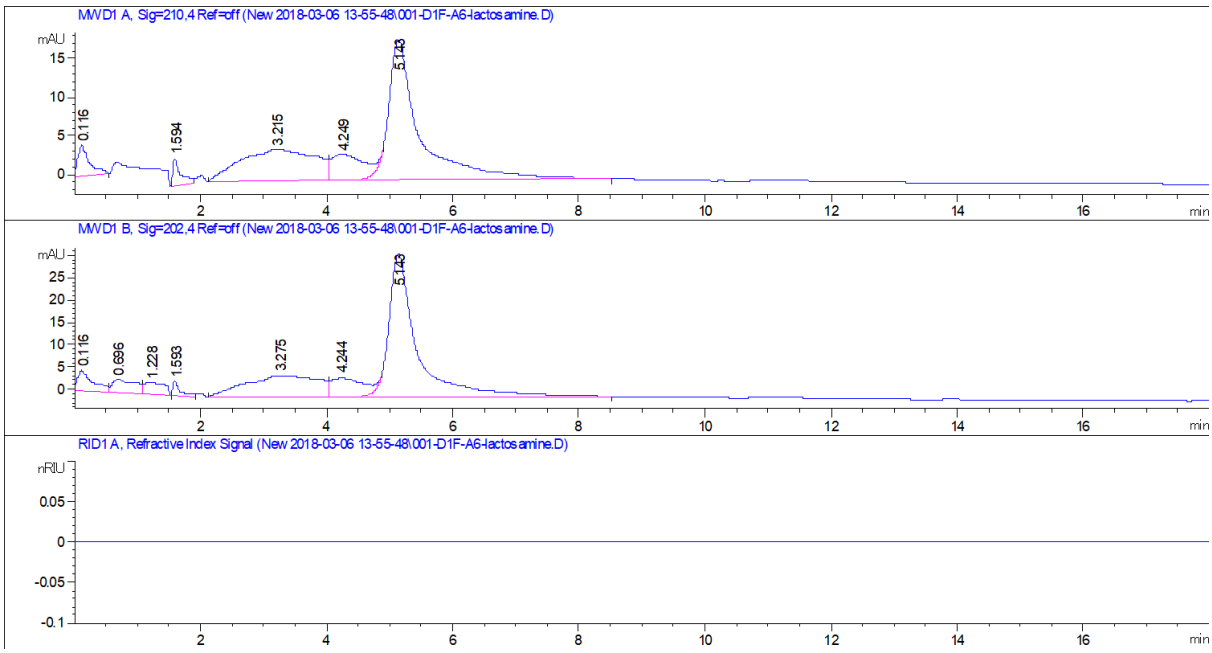

Figure S11: HPLC trace lactosamine. 1 mL/min flow rate. Elution time 5.143 min.